

GROUNDING THE “NOT”: SYMBOLIC REPRESENTATION OF NEGATION FOR LOGICAL REASONING IN VLMS

Anonymous authors

Paper under double-blind review

ABSTRACT

Despite their remarkable capabilities in natural language understanding, Vision-Language Models (VLMs) exhibit critical bottlenecks in fundamental logical reasoning, particularly in processing the logical operator of negation. This deficiency frequently results in self-contradictory predictions, where models fail to differentiate between a concept and its negation (A vs. $\neg A$), a phenomenon often observed as “affirmative bias” in visual contexts. In this work, we leverage Described Object Detection (DOD) as a rigorous testbed to evaluate and resolve these logical inconsistencies. To address this, we propose two primary contributions. First, we introduce COVAND, a dataset constructed via a deductive chain-of-thought (CoT) reasoning pipeline that synthesizes consistent, instance-grounded logical propositions. Second, we present NEGTOPE, a novel token merging module that acts as a symbolic representation mechanism. NEGTOPE directly mitigates the structural loss of logical operators caused by standard tokenization. By explicitly binding negation cues with their target operands (e.g., merging “not” and “girl” into a singular, structurally coherent \neg girl token), it preserves strict logical polarity at the input representation level. Evaluated on rigorous consistency benchmarks, our lightweight adaptation approach significantly reduces self-contradictory false positives and boosts NMS-AP by up to +10.8 points on OVDEval. This work demonstrates an effective framework for embedding symbolic logical operations into VLMs, paving the way for more reliable deductive reasoning in multimodal applications.

1 INTRODUCTION

Even state-of-the-art Vision-Language Models (VLMs) exhibit a critical failure in understanding negation due to an affirmative bias (Alhamoud et al., 2025). This bias reflects a model’s tendency to prioritize nouns while ignoring crucial negation cues. The issue is particularly pronounced in *described object detection* (DOD) (Xie et al., 2023; Schultze et al., 2023; Yao et al., 2024; Dang et al., 2023), a task requiring fine-grained compositional reasoning. As in Figure 1a, this bias causes models to treat phrases like “*person with skateboard*” and “*person without skateboard*” as semantically equivalent, leading to identical and incorrect detections. This failure extends to more complex logical structures, such as double negatives (e.g., “not” + “un-”). Since humans naturally use negation in natural communication (Sarabi & Blanco, 2016; Morante & Blanco, 2021; Beukeboom et al., 2020; Morante & Sporleder, 2012), failing to handle negation poses a serious barrier to real-world scenarios. This shortcoming can be particularly dangerous in safety-critical domains. For example, in medical imaging, misinterpreting the distinction between “*a tumor that is not malignant*” and “*a tumor that is malignant*” can lead to critical misdiagnoses. Therefore, bridging and improving negation understanding is an important step toward building robust VLM-based detection systems.

One key reason for the limited negation capability of VLMs is the lack of negated expressions in existing pre-training datasets. For example, large-scale datasets such as LAION-400M (Schuhmann et al., 2021) contain about 0.08% negation words (Park et al., 2025). Likewise, Flickr30k (Plummer et al., 2015), a widely used captioning dataset, exhibits only 0.04% negation words (Figure 1b). In contrast, negation is much more prevalent in real-world language. For instance, 13.76% of words in scientific papers (Szarvas et al., 2008) and 22.23% of words in Conan Doyle’s stories involve

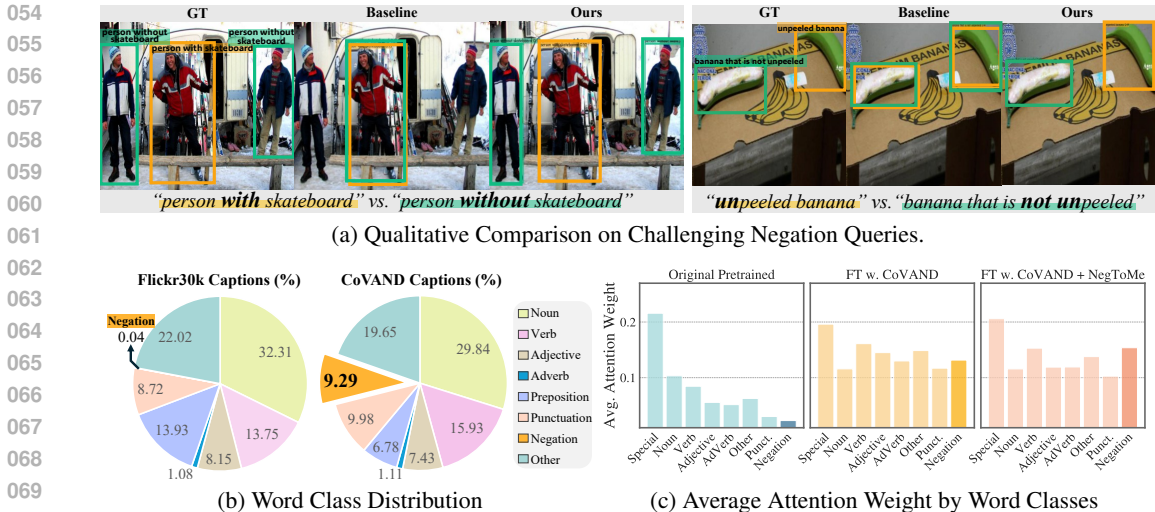


Figure 1: **Challenges with Negation Expressions.** (a) Standard VLMs exhibit an affirmative bias, failing to distinguish contradictory negation queries. This issue stems from two causes: (b) the scarcity of negation words in standard datasets and (c) the model’s tendency to assign low attention to negation cues. Our solutions, COVAND and the NEGToME, directly address both problems.

negation (Morante & Daelemans, 2012). This imbalance results in VLMs that are poorly equipped to learn or attend to negation semantics.

To mitigate this limitation, we introduce a chain-of-thought with VQA alignment for negation detection dataset (CoVAND). It is a negation-focused training dataset constructed via chain-of-thought (CoT) reasoning and VQA-based caption alignment. To construct CoVAND, we first extract both present and absent attributes from object regions. For each region, we then generate matched positive and negative captions using a CoT approach, followed by semantic verification using a VQA module. This process ensures each caption precisely reflects the presence or absence of key attributes, resulting in high-quality negation data pairs. As a result, our dataset provides a rich resource with 9.29% of negation words, a frequency 100× higher than that of typical datasets.

In addition to data-related factors, we observe that negation tokens receive notably lower attention weights, suggesting that current VLM detectors architecturally ignore or undervalue negation cues, as shown in Figure 1c. To counteract the low attention given to negation cues, the core of our method is NEGToME, our novel text token merging module. It is designed to solve a key problem where standard tokenization often fragments phrases, separating negation cues (e.g., “not”) from the attributes they modify (e.g., “lying”). NEGToME addresses this by first merging these fragmented tokens into a single, coherent phrase. Through this binding, the negated concept of “not lying” can be learned as semantically distinct from “lying”. This step strengthens the role of the attribute by ensuring it is always interpreted within its negated context. Crucially, this merged representation is enhanced with a negation-aware boost, explicitly amplifying the negated signal to ensure its polarity is preserved for downstream fusion. To our knowledge, this is the first work to employ a boosted token merging strategy for preserving semantic polarity in VLM-based detection.

To ensure the model effectively uses this enhanced text representation, we combine NEGToME with a highly targeted application of Low-Rank Adaptation (LoRA). Our layer-wise attention analysis revealed that the negation signal dissipates before reaching the final decision-making blocks. Therefore, we apply LoRA to the deep cross-attention layers, the core of multimodal compositional understanding (Laurençon et al., 2024; Hertz et al., 2022). Together, this strategy modifies less than 0.1% of the model’s parameters yet achieves a significant improvement in negation comprehension.

Our approach achieves state-of-the-art performance with 6.6 mAP on D³ dataset, with 7.2 mAP improvement specifically on the challenging absence subset. In particular, our method not only increases the NMS-AP metric by 10.8 mAP but also reduces the false positive rate by 19.1%, demonstrating its enhanced ability to distinguish between contradictory queries. Importantly, these results are consistently observed across multiple distinct evaluation datasets, despite the model being

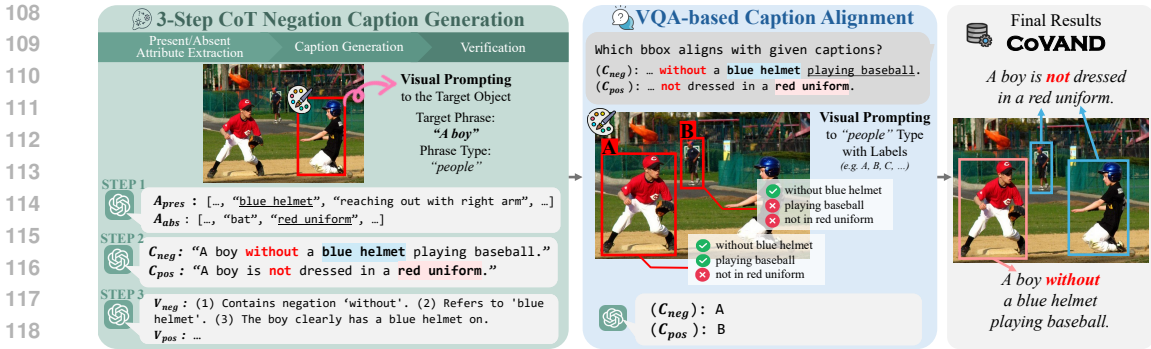


Figure 2: **Dataset Generation Pipeline of the COVAND.** Our method first generates negation-focused captions for visually prompted regions using a three-step CoT process, then aligns each caption with the correct bounding box via VQA-based reasoning to ensure semantic correspondence.

trained solely on COVAND. This highlights the strength of our approach and its superior generalization capability to unseen data and negation patterns.

Our work represents an initial yet substantial step toward robust negation understanding with the following key contributions:

- Our work presents COVAND, a systematically generated dataset focusing on negation, to bridge a critical gap within existing multimodal benchmarks.
- We propose a novel adaptation recipe with NEG-TOME, our text token merging module that introduces a negation-aware boost to preserve semantic polarity.
- We achieve consistent gains across benchmarks, including +7.2 mAP on D³ absence subset and +10.8 mAP on the NMS-AP metric in OVDEval’s negation subset, demonstrating effective generalization to real-world negation scenarios.

2 COVAND: DATASET GENERATION

To address the scarcity of negation data, we present COVAND, a region-grounded negation dataset constructed through a multi-stage pipeline. As shown in Figure 2, the curation process consists of CoT caption generation followed by VQA-based alignment. Through this process, our approach generates new high-quality captions that enable it to cover not only object existence but also diverse attribute-based negations, such as actions, relationships, and spatial properties. In this way, COVAND provides fine-grained, compositional supervision that trains detectors more robustly than only injecting templated or caption-level negations (Alhamoud et al., 2025; Park et al., 2025).

2.1 VISUAL PROMPTING WITH BOUNDING BOXES

Before caption generation, we apply visual prompting (Cai et al., 2024) to overlay a marker on the image. The marker specifies the region to describe and directs the CoT model’s attention to that area. We apply this technique to bounding boxes in the Flickr30k Entities dataset (Plummer et al., 2015). For each image, we randomly choose two boxes linked to meaningful objects and exclude any box that spans a large background area to avoid ambiguity. Each selected region is then highlighted with a red bounding box and serves as an input image for region-grounded caption generation.

2.2 THREE-STEP CHAIN-OF-THOUGHT CAPTION GENERATION

We generate region-grounded paired negation captions through a three-step CoT process using GPT-4o (Hurst et al., 2024). We provide an explicit sequence that ensures consistent quality, rather than leaving it to the model’s decision. The design follows the multi-step reasoning strategy of LLMs, where a complex visual query is split into ordered subtasks that improve factual accuracy and transparency. The input prompt for caption generation shows the image with a red bounding box, a target phrase such as “a boy” in “person” type. These cues fix the subject within the highlighted area and guide each reasoning step. The three steps are detailed below.

Step 1: Present and Absent Attribute Extraction. For each visually prompted region, we extract two sets of attributes: (1) *Present Attributes* (A_{pres}), consisting of attributes visibly present within the bounding box (e.g., colors, actions, relationships, actions, etc.), and (2) *Absent Attributes* (A_{abs}), representing relevant but missing attributes that could reasonably be expected. This rich attribute pool is the key novelty that lets our pipeline create attribute-level negations, which are far beyond the object-level attributes used in prior approaches (Alhamoud et al., 2025).

Step 2: Negative and Positive Caption Generation. We generate two types of paired captions using the extracted attributes:

- *Negative Caption* (C_{neg}): Incorrectly describes an attribute in A_{pres} as absent (e.g., “A man without a hat” when “hat” $\in A_{pres}$).
- *Positive Caption* (C_{pos}): Correctly describes an attribute in A_{abs} as absent (e.g., “A woman without a red hoodie” when “red hoodie” $\in A_{abs}$).

Each caption includes negation cues such as “no”, “not”, “never”, “without”, the prefix “un-”, or the contraction “n’t”. The cue list is open to keep language natural and diverse.

Step 3: Verification. To ensure semantic consistency, we verify that C_{pos} accurately describes the region while C_{neg} contradicts it by asking GPT-4o. We also check whether generated captions contain negation words and attributes from step 1. If the pair fails on the test, it discards invalid captions and repeats caption generation until a valid pair appears or the retry limit is reached. This iterative guard preserves semantic integrity and keeps the quality of the overall dataset.

2.3 VQA-BASED CAPTION ALIGNMENT

The CoT stage produces a positive caption C_{pos} and a negative caption C_{neg} for each randomly chosen target box. However, label noise may still occur since another object of the same phrase type can also fit the captions. In Figure 2, for example, a person marked with “A” in the image could satisfy C_{neg} , even though it is not the designated target, which causes label noise. To eliminate this ambiguity, we add a dedicated region-level VQA alignment step.

First, we draw alphabetical labels on every box that shares the phrase type of the target. The target box stays unlabelled because it has already passed the in-context verification step. To determine the final alignment, we ask a VQA model two separate questions: “Which labelled box aligns with C_{pos}/C_{neg} ?”. Then, the VQA model simply answers with overlaid letters on the input images. While prior work used VQA for coarse, image-level validation (Park et al., 2025), their approach fails to resolve which specific instance a caption refers to. Our region-level alignment stage solves this ambiguity by requiring the VQA model to match each caption to a specific, visually-labeled bounding box, thereby delivering a more region-level ground truth.

Through this multi-stage process combining CoT reasoning and VQA alignment, COVAND provides rich training signals for negation understanding. We generate 91,110 captions with 23,876 images. In particular, our dataset exhibits approximately 9.29% negation word frequency, significantly higher than existing datasets like Flickr30k (0.04%). Detailed examples in Appendix A.

3 FINE-TUNING WITH NEGATION-SENSITIVE TEXT TOKEN MERGING

Our method addresses the two root causes of negation blindness: token fragmentation and low attention on negation cues. We propose a lightweight adaptation recipe that integrates our novel text token merging module, NEG-TOME, with a targeted application of LoRA as in Figure 3.

3.1 NEGATION LORA ADAPTER

We apply LoRA following (Hu et al., 2022) with two key enhancements for vision-language fusion. Given frozen base weights $W_q, W_v \in \mathbb{R}^{d \times d}$ in cross-attention layers, we inject parallel adapters with an activation layer. Let $\sigma(\cdot)$ denote ReLU (Agarap, 2018) and let $A_q, A_v \in \mathbb{R}^{r \times d}$ and $B_q, B_v \in \mathbb{R}^{d \times r}$ be the trainable low-rank matrices. For an input $x \in \mathbb{R}^d$ we obtain

$$q = W_q x + \alpha B_q \sigma(A_q x), \quad v = W_v x + \alpha B_v \sigma(A_v x), \quad (1)$$

where $W_q, W_v \in \mathbb{R}^{d \times d}$ are the frozen base weights and α scales the LoRA update.

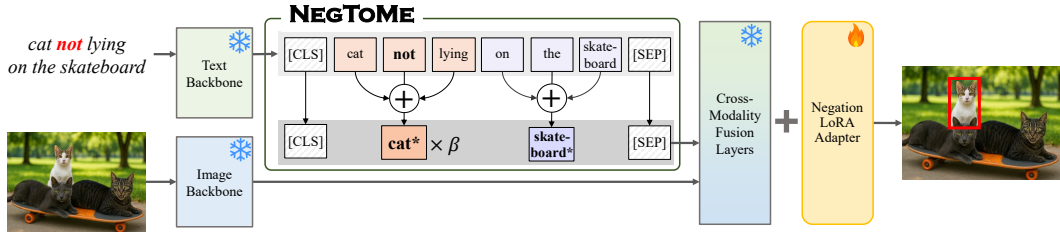


Figure 3: **Overview of Training Pipeline.** The input image and captions of COVAND are encoded by frozen backbones. NEGTOme assigns higher importance to negation cues in the text, and the LoRA adapter enables accurate localization of objects described by negated queries.

3.2 NEGTOme: SEMANTIC TEXT TOKEN MERGING FOR NEGATION UNDERSTANDING

Motivation. While fine-tuning with negation-rich data can partially alleviate affirmative bias, it does not address a more fundamental flaw embedded in the model’s tokenization process. Standard tokenizers inherently fragment phrases, separating negation cues (e.g., “not”) from the words they modify (e.g., “lying”). This structural separation effectively causes the model to treat the phrase “not lying” as semantically equivalent to “lying”, as the attention weight of the isolated negation tends to be ignored. To rectify this intrinsic information loss, we introduce NEGTOme. It moves beyond data-level fixes to structurally ensure that a negated concept like “cat not lying” is represented as a single semantic unit, fundamentally distinct from {“cat”, “not”, “lying”}.

Text Token Merging. The caption is first split into sub-tokens $\mathcal{T} = \{t_1, \dots, t_n\}$ by a standard tokenizer. To merge the tokens, an off-the-shelf parser then groups these tokens into disjoint phrase sets $\mathcal{P} = \{\mathcal{P}_1, \dots, \mathcal{P}_m\}$ where $m < n$. For every phrase $\mathcal{P}_i \subseteq \mathcal{T}$, we compute one representative embedding by taking the normalized weighted average using fixed importance weights γ_j of the sub-token vectors inside the phrase and replacing the original vectors with this average.

Negation-aware Boost. After merging, let \mathcal{P}_{neg} be the phrase containing a cue (not, no, without, un-, etc.), and $\mathcal{I}_{\text{neg}} = \{j \mid t_j \in \mathcal{P}_{\text{neg}}\}$ its index set. We assign a larger weight to the negation cue:

$$\bar{t}_{\text{neg}} = \frac{\sum_{j \in \mathcal{I}_{\text{neg}}} \gamma_j t_j}{\sum_{j \in \mathcal{I}_{\text{neg}}} \gamma_j}, \quad \gamma_j = \begin{cases} \beta & \text{if } t_j \text{ is the negation cue,} \\ 1 & \text{otherwise,} \end{cases} \quad \beta > 1. \quad (2)$$

The negation boosting factor β amplifies the cue so that the merged embedding explicitly retains the negated meaning, improving polarity reasoning without increasing sequence length.

Effect of Negation Boost on Representations. Suppose the encoder maps a caption of n sub-tokens to vectors $h_1, \dots, h_n \in \mathbb{R}^d$. We write h_c for the vector of the negation cue (e.g. “not”) and h_p for the vector of the predicate it modifies (e.g. “moving”). With vanilla mean pooling, the sentence embedding is $\bar{h} = \frac{1}{n} \sum_{i=1}^n h_i$, so the cue contributes only $s_{\text{single}} = \langle v, h_c \rangle / n$ to any linear probe $v \in \mathbb{R}^d$. After applying NEGTOme, the merged representation of the negated phrase becomes $h_{\text{neg}} = \frac{\beta h_c + h_p}{\beta + 1}$ and the pooled vector gives $s_{\text{merge}} \geq \frac{\beta}{\beta + 1} \langle v, h_c \rangle / m$. Hence

$$\frac{s_{\text{merge}}}{s_{\text{single}}} \geq \frac{\beta}{\beta + 1} \cdot \frac{n}{m}, \quad 1 \leq m < n, \quad (3)$$

so the cue’s influence is amplified by at least the factor $\frac{\beta}{\beta + 1} \cdot \frac{n}{m}$. This gain aligns with the larger attention weights observed in Figure 1c and Figure S18, and experimentally show higher mAP.

4 EXPERIMENTS

4.1 EXPERIMENTAL SETUPS

Datasets. DOD requires resolving compositional descriptions as in Figure 4a. To rigorously assess our model’s ability to overcome the affirmative bias inherent in VLMs, we select two benchmarks specifically designed to challenge negation understanding. We evaluate our method on two challenging DOD benchmarks for negation detection in VLMs. *Described Object Detection (D³)* (Xie et al.,

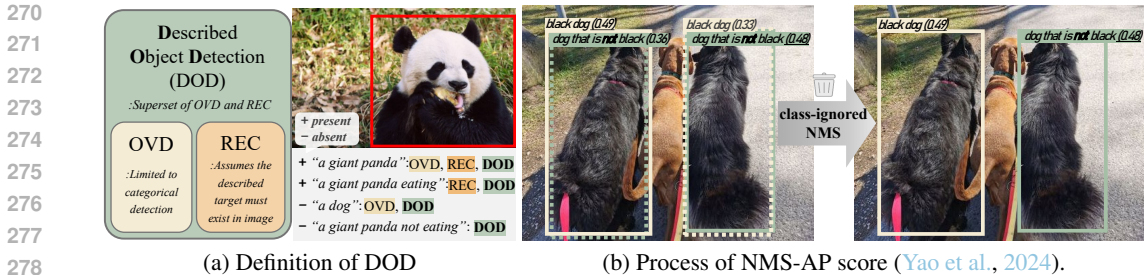


Figure 4: Definition of Task and Metric.

(2023) introduces three evaluation protocols. *Pres* is a subset of 316 presence descriptions, *Abs* is 106 absence descriptions, and *Full* is an evaluation across all 422 descriptions. For *OVDEval Negation Subset* (Yao et al., 2024), we report both standard AP and the NMS-AP. The standard AP score can be misleadingly inflated when a model, confused by fragmented tokens, predicts overlapping boxes for contradictory pairs like “black dog” and “dog that is not black”. In contrast, NMS-AP (Yao et al., 2024) applies stricter filtering by removing overlapping predictions on contradictory pairs with $\text{IoU} > 0.5$, effectively penalizing affirmative bias and accurately measuring negation understanding (Figure 4b). Additionally, we employ a practical yet challenging evaluation by performing class-ignored NMS separately after predicting each caption individually. (see the Appendix F.1.)

Implementation Details. We implement parameter-efficient fine-tuning through LoRA (Hu et al., 2022) applied to the deep cross-attention layers in the vision-language fusion module with $r = 4$. VLM-based detectors are trained for 5,000 iterations with a batch size of 24 for the Grounding DINO model, and 6,000 iterations with a batch size of 4 for the APE-Ti model. Training is conducted on two NVIDIA A6000 GPUs with mixed precision with a learning rate of 5×10^{-4} . Qwen-2.5-VL (Bai et al., 2025) is trained for 1 epoch batch size of 32 with a learning rate of 5×10^{-5} . All models are only trained with the CoVAND dataset using the AdamW optimizer (Loshchilov & Hutter, 2017), freezing all backbone parameters except the LoRA layers. For NEGTOme, we use spaCy for the parser and set the negation boost factor $\beta = 2.0$. More details in the Appendix B.

4.2 EXPERIMENTAL RESULTS

Quantitative Results. As shown in Table 1, even powerful Multimodal Large Language Models (MLLMs) struggle with the D^3 benchmark. SoTA models like SPHINX-7B (Lin et al., 2023) and Qwen-2.5-VL-3B (Bai et al., 2025) achieve low performance on the full set (10.6 and 18.6 mAP, respectively), and their slow inference makes them impractical for many detection scenarios. In contrast, our lightweight adaptation recipe significantly boosts the performance of strong detector baselines. When applied to Grounding-DINO, our method improves the overall mAP by +6.6 points, with a notable gain of +7.2 mAP on the challenging absence subset. This performance gain is direct evidence of a more robust understanding of semantic polarity. Baseline models often generate

Table 1: Evaluation on the D^3 benchmarks. Descriptions categorized by length; *S* for 1-3, *M* for 4-6, *L* for 7-9, and *XL* for 10+ words. *Pres* refers to present and *Abs* refers to absence subset.

Method	Architecture			D^3 (default)			D^3 (by length of texts)			
	Backbone	Text Encoder	Detection Head	Full	Pres	Abs	S	M	L	XL
OFA-L	ResNet-101+ViT	BART	Seq2Seq	4.2	4.1	4.6	4.9	5.4	3.0	2.1
OWL-ViT-L	ViT-L	CLIP	OWL-ViT	9.6	10.7	6.4	20.7	9.4	6.0	5.3
SPHINX-7B	CLIP,DINO-v2, Q-Former	LLaMA-2	-	10.6	11.4	7.9	16.8	13.8	5.6	3.1
OFA-DOD	ResNet-101+ViT	BART	Seq2Seq	21.6	23.7	15.4	23.6	22.6	20.5	18.4
GLIP-T	Swin-T	BERT	DyHead	19.1	18.3	21.5	22.4	22.0	16.6	10.6
+ GEN				21.4	20.6	23.7	28.1	24.5	17.4	11.5
+ W2S				26.0	25.6	27.1	-	-	-	-
FIBER-B	Swin-B	RoBERTa-B	DyHead	22.7	21.5	26.0	30.1	25.9	17.9	13.1
+ GEN				26.0	25.2	28.1	35.5	29.7	20.5	14.2
+ W2S				26.5	26.0	27.7	-	-	-	-
G-DINO-B	Swin-B	BERT	DINO	20.7	20.1	22.5	22.6	22.5	18.9	16.5
+ Ours				27.3	26.4	29.7	29.9	29.5	25.2	21.3
($\uparrow \Delta$)				(+6.6)	(+6.3)	(+7.2)	(+7.3)	(+7.0)	(+6.3)	(+4.8)
APE-Ti	ViT-Ti	CLIP	DETA	29.1	29.9	26.9	31.1	31.9	27.4	21.4
+ Ours				32.5	32.9	31.5	33.2	35.3	31.3	25.4
($\uparrow \Delta$)				(+3.4)	(+3.0)	(+4.6)	(+2.1)	(+3.4)	(+3.9)	(+4.0)
Qwen-2.5-VL-3B	ViT-H	Qwen-2.5	-	18.6	18.5	19.2	18.2	20.7	17.0	16.0
+ Ours				22.2	22.8	20.6	19.8	25.8	20.2	17.8
($\uparrow \Delta$)				(+3.6)	(+4.3)	(+1.4)	(+1.6)	(+5.1)	(+3.2)	(+1.8)

false positives because they fail to distinguish between conceptually opposite phrases like “with a hat” and “without a hat”. As a specific absence scenario, when prompted with “a person without a hat” in an image where everyone is wearing one, they would incorrectly detect a person. Our tokenizer modification, NEG-TOME, resolves this by forcing the model to process the negated phrase as a single semantic unit with distinct polarity, enabling it to correctly reject such invalid instances. Similarly, on APE-Ti, we achieve a +4.6 mAP improvement on the absence subset, demonstrating an enhanced ability to reject non-existent objects. Notably, these gains are comparable to computationally expensive, large-scale fine-tuning methods (Zhao et al., 2024a; Park et al., 2024b) while updating less than 0.1% of the model’s parameters only with our COVAND dataset. The improvements are also consistent across all description lengths, validating the robustness of our approach. Furthermore, preliminary experiments demonstrate the generalizability of our method to MLLMs, with an improvement of +3.6 mAP on Qwen-2.5-VL-3B.

Even powerful SoTA MLLMs struggle on the challenging OVDEval-Negation subset, demonstrating that simply applying a large-scale model is not a sufficient solution for negation. Notably, as shown in Table 2, the powerful Qwen-2.5-VL-7B underperforms the much smaller Grounding-DINO baseline, highlighting the difficulty of the task. In contrast, our lightweight adaptation recipe yields significant performance gains across all tested architectures, particularly on the stricter NMS-AP metric. Our method boosts the Grounding-DINO by a substantial +10.8 mAP in NMS-AP and improves the Qwen-2.5-VL-3B by +7.3 in mAP and +3.8 in NMS-AP. For the MLLM, the substantial AP gain is significant because it enhances both negation reasoning and foundational localization, a typical weakness of such models. Further results, including a detailed comparison with two-stage post-hoc VQA with MLLM and a full evaluation across all OVDEval subsets, are available in Appendix E and F.

Table 2: Results on OVDEval-Negation. † means reproduced AP.

	AP	NMS-AP
G-DINO-B†	54.0	36.8
+ Ours	57.2	47.6
(↑ Δ)	(+3.2)	(+10.8)
APE-Ti	50.5	32.3
+ Ours	54.1	33.5
(↑ Δ)	(+3.6)	(+1.2)
Qwen-2.5-VL-7B	37.8	35.9
Qwen-2.5-VL-3B	34.6	31.3
+ Ours	41.9	35.1
(↑ Δ)	(+7.3)	(+3.8)

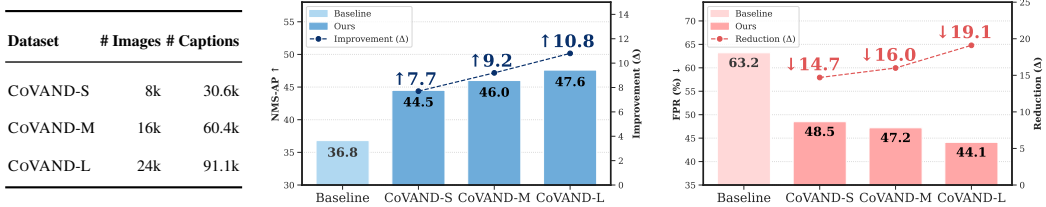


Figure 5: Dataset Statistics and Performance Scaling. (a) Statistics for our three COVAND splits. (b) Bar plots with blue refer to NMS-AP and pink refer to FPR (lower is better).

Dataset Scalability. Figure 5 presents our scalability analysis of the dataset on the OVDEval-Negation subset. We observe a consistent improvement as we scale the COVAND dataset from small to large. Specifically, NMS-AP improves from 44.5 to 47.6, while the FPR decreases from 48.5% to 44.1%, which is a total reduction of 19.1 points from the baseline. This trend of simultaneously improving NMS-AP, a metric that penalizes contradictory predictions, while lowering FPR, which measures the failure to reject absent objects, shows the effectiveness of our approach.

Qualitative Results. Figure 6 presents qualitative results from the OVDEval dataset comparing our fine-tuned Grounding DINO model against the baseline. The baseline model often exhibits a strong affirmative bias, frequently collapsing contradictory captions into the same prediction. Our model, however, successfully handles these complexities across various patterns. For instance, it accurately identifies the “cow without looking at the camera” and the “horse that is not urinating”, proving it can ground negation in complex contexts. Moreover, for “banana that is not unpeeled”, it correctly identifies the peeled banana by resolving the “not” + “un-” double negative as in Figure 1a. Our model sometimes fails to detect every target instance, for example “pizza that is not complete”, its predictions are a marked improvement over the baseline, which provides completely unreliable detections for both queries. Together, these examples show that our method achieves a more compositional understanding of negation. Further qualitative results on OVDEval and D³ are presented in Figure S23–S24 and Figure S25–S27, respectively.

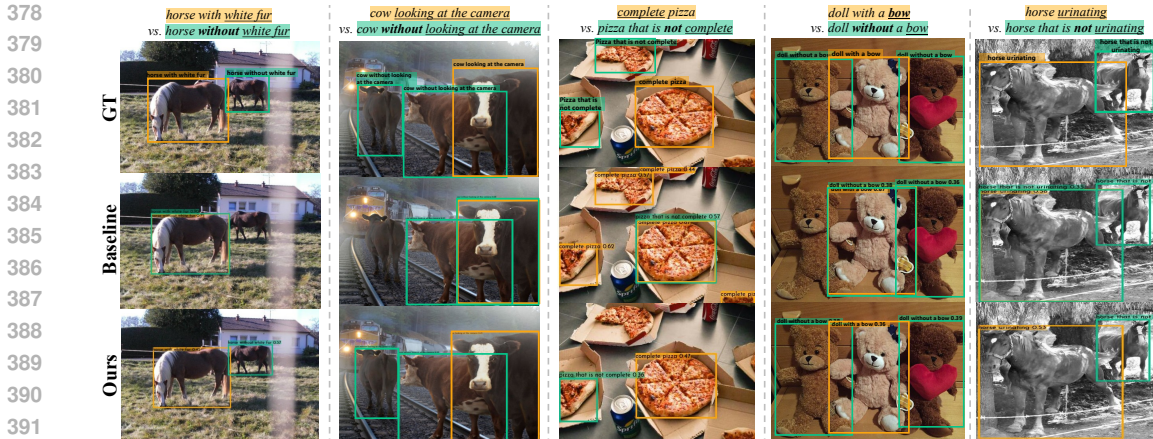


Figure 6: **Qualitative Comparison on the OVDEval Negation Subset.** Our model correctly distinguishes the polarity of contradictory caption pairs, overcoming the baseline’s affirmative bias.

Table 3: **Ablation Study.** Best in blue and worst in red. LoRA adapters are inserted at three fusion-block depths: shallow (blocks 0–2), strided (1, 3, 5), and deep (3–5).

Training Data	Settings			OVDEval (Negation Subset)					D ³			
	LoRA Placement	NEGToME	β	AP	NMS-AP	AR	NMS-AR	↓FPR	Full	Pres	Abs	↓FPR
Pretrained Weight				54.0	36.8	20.5	14.7	63.2	20.7	20.1	22.5	67.2
Flickr30k	shallow	✗	–	55.9	38.5	21.7	15.2	61.3	18.4	18.2	23.0	66.5
Flickr30k	strided	✗	–	54.8	36.5	20.5	14.1	62.6	20.9	19.9	24.0	68.2
Flickr30k	deep	✗	–	53.7	31.8	20.7	12.8	59.9	22.0	21.0	24.8	67.8
CoVAND-S	shallow	✗	–	46.8	31.5	21.9	14.8	56.0	18.5	17.6	21.0	63.9
CoVAND-S	strided	✗	–	52.8	43.9	20.0	17.1	49.0	20.1	19.2	22.9	63.4
CoVAND-S	deep	✗	–	55.4	41.8	21.4	18.0	48.6	24.2	23.0	27.0	64.0
CoVAND-S	deep	✓	1.0	57.8	43.8	24.0	19.6	50.8	25.7	25.1	27.3	63.7
CoVAND-S	deep	✓	2.0	58.7	44.5	24.1	19.2	48.5	26.2	25.4	28.2	63.3

4.3 ABLATION STUDY

Our ablation study, summarized in Table 3, reveals the impact of each component, with attention diagnostics in Figure S18 in the Appendix providing a clear mechanism for the improvements. Placing LoRA adapters in the deep fusion blocks consistently outperforms shallow. This is because deep placement maintains elevated attention on negation tokens in the later blocks where decisions are formed, whereas the effect of shallow placement dissipates too early. Furthermore, training with CoVAND dataset yields substantial gains over generic captions, demonstrating its value for both accuracy and generalization. Finally, adding NEGToME with its negation boost factor provides large gains, such as a +2.7 improvement in NMS-AP. This trend is mirrored on the D³ benchmark. While using our CoVAND dataset alone yields a +2.2 mAP improvement over the baseline, NEGToME adds a further +2.0 mAP on top. This near-equal contribution highlights that our token merging strategy is as impactful as the dataset itself. The attention analysis further confirms that NEGToME directly causes this improvement by increasing attention to the negated phrase.

4.4 ZERO-SHOT DOWNSTREAM EVALUATION OF SEMANTIC COMPREHENSION.

To verify our method achieves a semantic understanding of negation that generalizes beyond detection, we evaluate it on the NegBench COCO subset of Multiple Choice Question (MCQ) benchmark (Alhamoud et al., 2025). This task requires the model to select the most accurate caption for an image from four options. These options include three subsets: ‘Positive’ correctly affirming present objects (e.g., “A and B”), ‘Negative’ correctly negating absent ones (e.g., “not B”), and ‘Hybrid’ that combine both types (e.g., “A but not B”). In a zero-shot setting, we select the caption that produces the highest max-logit score when grounded in the image. As shown in Table 4, our method improves accuracy over the baseline with a +10.86% improvement.

Table 4: **Results on the NegBench Multiple Choice Question (MCQ) benchmark.**

Model	Overall Acc.	Positive	Negative	Hybrid
CLIP-OpenAI	16.27 %	—	—	—
NegCLIP	10.21 %	—	—	—
G-DINO-B	21.69 %	27.36 %	13.37 %	23.71 %
+ Ours	32.55 %	46.85 %	23.37 %	26.64 %
($\uparrow \Delta$)	(+10.86)	(+19.49)	(+10.00)	(+2.93)

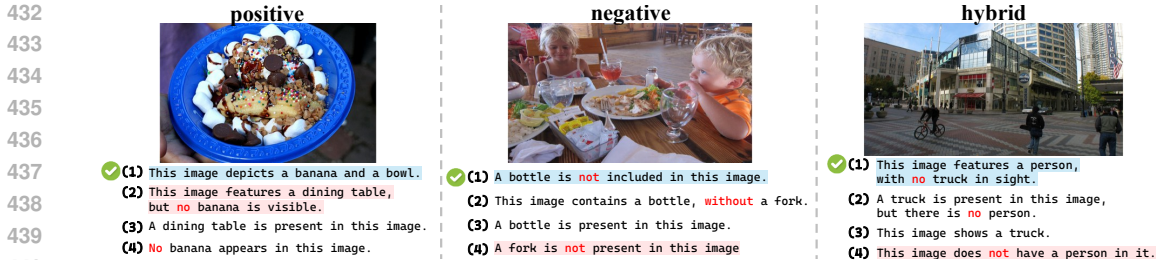


Figure 7: **Qualitative Comparison on the NegBench MCQ Benchmark.** Captions with green checkmark ✓ is GT, pink refer to **Baseline**, and blue refer to **Ours**.

This result provides strong evidence that our approach enhances a robust understanding of negation. We present qualitative examples in Figure 7 and in Appendix H.

4.5 ZERO-SHOT GENERALIZATION ON BIOMEDICAL DOMAIN

To validate that our method learns a robust mechanism of negation processing rather than merely memorizing specific object-negation pairs from the COVAND dataset, we conduct a zero-shot evaluation on the biomedical domain. We utilize the FG-CXR dataset (Pham et al., 2024), a fine-grained chest X-ray benchmark that aligns radiologist gaze with diagnostic reports. This domain poses a severe generalization challenge due to the drastic shift in visual features (grayscale X-rays) and a distinct linguistic taxonomy of negation (e.g., “normal”, “clear”, “no findings”).

Unlike standard captioning benchmarks, FG-CXR maps diagnostic sentences to specific anatomical regions (e.g., heart, upper left lung). We formulate the evaluation as a zero-shot binary discrimination task. Specifically, we flatten the dataset to evaluate every valid anatomical region individually by extracting its ground truth (GT) diagnosis. To strictly test negation understanding, we generate a hard negative contradiction for every GT sentence by syntactically flipping its polarity using a rule-based approach. This transformation encompasses state negations (e.g., “The left lung is possibly normal” → “... abnormal”), the absence of findings (e.g., “No pleural effusion” → “Pleural effusion is present”), and disease assertions (e.g., “Opacity in the right lung” → “No opacity...”). We report accuracy as our primary metric, considering a prediction correct if the model assigns a higher matching score (maximum logit) to the GT caption than to the hard negative caption, given the corresponding visual region.

Table 5: **Zero-shot Results on FG-CXR.**

Method	Accuracy
Baseline (G-DINO-B)	54.86%
+ Ours (NEG-TOME)	62.55%

The results of this cross-domain evaluation are presented in Table 5. The baseline model achieves an accuracy of 54.86%, which is only marginally above random chance. This confirms that standard VLMs struggle deeply with medical negation, often failing to distinguish “normal” from “abnormal” even when visual features are highly distinct. In contrast, our method achieves 62.55% (+7.69%), marking a substantial improvement. Since our model is never exposed to medical images or jargon during fine-tuning, this performance gain cannot be attributed to memorizing in-domain data. Instead, it demonstrates that NEG-TOME effectively structuralizes the binding between negation cues (e.g., “no”, “normal”) and their targets, allowing the model to successfully generalize this fundamental reasoning mechanism to entirely unseen domains.

5 RELATED WORK

5.1 OBJECT DETECTION

OVD extends classical detectors to arbitrary text labels (Zareian et al., 2021; Yao et al., 2022; Kim et al., 2023a). Methods such as GLIP (Li et al., 2022), and APE (Shen et al., 2024) fuse language either in the detection head, in the backbone, or in a task-general prompt module, and achieve strong zero-shot performance. REC adds compositional phrases. Grounding DINO (Liu et al., 2024b) proposes DETR-style decoders that localize the described object without category supervision. Despite this progress, REC models still assume the target exists and therefore struggle to reject absent or

negated descriptions. DOD (Xie et al., 2023) generalizes OVD and REC by requiring the detector to decide both existence and location. Benchmarks such as D³ and OVDEval (Yao et al., 2024) reveal a low in accuracy on absence or negation subsets. It confirms that current VLMs often have an affirmative bias on negation cues. MLLM (Lin et al., 2023; Bai et al., 2025) have recently been applied to DOD, but their accuracy fails to surpass that of VLM-based detectors, their performance on negation remains low, and their inference speed is incompatible with real-time detection scenarios.

5.2 NEGATION UNDERSTANDING IN VISION-LANGUAGE MODELS

CLIP-based studies such as NegBench (Alhamoud et al., 2025) reveal the affirmative bias that state-of-the-art VLMs often treat “dog” and “not dog” identically; subsequent fixes like Negation-CLIP (Park et al., 2025) simply augment pre-training with template-level negation pairs and thus miss context-dependent or region-grounded cases. We instead build a fine-grained dataset with CoT reasoning and VQA alignment, producing positive and negative caption pairs that are grounded to target boxes, and show that this richer supervision transfers to multiple architectures beyond CLIP.

5.3 TEXT TOKEN-LEVEL MERGING

Token Merging (ToMe) (Bolya et al., 2022) merges similar image tokens to accelerate inference without sacrificing accuracy. ToMe is extended to diffusion and grounding models, where token merging based on semantic phrase is introduced to mitigate the loss of modifier information (Hu et al., 2024; Li et al., 2024b). In the context of OVD, there have been attempts to merge image tokens (Su et al., 2024; Norouzi et al., 2024), but the merging of text tokens has been unexplored. Previous studies on text token merging have primarily focused on diffusion models, particularly in text-to-image generation (Hu et al., 2024). In this work, we are the first to explore text token merging in detection models and empirically demonstrate its feasibility and effectiveness.

5.4 COMPOSITIONAL REASONING IN VISION-LANGUAGE TASKS

A comprehensive survey on compositional visual reasoning (Ke et al., 2025), establishing core definitions and theoretical foundations. The survey identifies key requirements for compositionality: (1) *primality* identifying atomic concepts, (2) *compositionality* systematically combining concepts, and (3) *systematicity* applying compositional rules consistently across novel scenarios. The survey emphasizes that compositional reasoning provides advantages in cognitive alignment, semantic fidelity, robustness, interpretability, and data efficiency. Notably, it highlights that vision-language models struggle with compositionality due to training data bias toward positive instances and the parallel feature processing architecture, a challenge directly addressed by COVAND.

Recent analysis reveals that VLMs exhibit the “binding problem” (Campbell et al., 2024)—fundamental failures in reliably associating perceptual features with correct visual referents, particularly in multi-object scenarios. This limitation mirrors cognitive science findings on rapid feedforward processing in human brains. Addressing this binding problem through structured spatial reasoning (e.g., horizontal lines and sequential scanning prompts) yields substantial improvements across visual reasoning tasks (Izadi et al., 2025), demonstrating that explicit compositional structure enhances multi-object understanding.

6 CONCLUSION

This work presents a comprehensive solution to the affirmative bias that hinders negation understanding in VLMs by addressing its two root causes. To resolve data scarcity, we introduce COVAND, a systematic pipeline using CoT reasoning and VQA-based alignment to generate high-quality, instance-grounded negation data. To counteract the model’s architectural tendency to ignore negation cues, we propose NEG-TOME, a novel module that, to our knowledge, is the first to use a negation-aware boost to preserve semantic polarity in detection tasks. Our parameter-efficient recipe integrates these contributions to achieve substantial gains on challenging negation benchmarks and demonstrate strong generalization across VLM-based detectors and MLLMs, marking a significant step towards VLMs that can understand not only what is present, but also what is absent.

BIBLIOGRAPHY

- 540
541
542 Amro Abbas, Kushal Tirumala, Dániel Simig, Surya Ganguli, and Ari S Morcos. Semdedup: Data-
543 efficient learning at web-scale through semantic deduplication. *arXiv preprint arXiv:2303.09540*,
544 2023.
- 545 Abien Fred Agarap. Deep learning using rectified linear units (relu). *arXiv preprint*
546 *arXiv:1803.08375*, 2018.
- 547 Paul Albert, Frederic Z Zhang, Hemanth Saratchandran, Cristian Rodriguez-Opazo, Anton van den
548 Hengel, and Ehsan Abbasnejad. Randlora: Full-rank parameter-efficient fine-tuning of large mod-
549 els. *arXiv preprint arXiv:2502.00987*, 2025.
- 550
551 Kumail Alhamoud, Shaden Alshammari, Yonglong Tian, Guohao Li, Philip Torr, Yoon Kim,
552 and Marzyeh Ghassemi. Vision-language models do not understand negation. *arXiv preprint*
553 *arXiv:2501.09425*, 2025.
- 554
555 Shuai Bai, Keqin Chen, Xuejing Liu, Jialin Wang, Wenbin Ge, Sibao Song, Kai Dang, Peng Wang,
556 Shijie Wang, Jun Tang, Humen Zhong, Yuanzhi Zhu, Mingkun Yang, Zhaohai Li, Jianqiang Wan,
557 Pengfei Wang, Wei Ding, Zheren Fu, Yiheng Xu, Jiabo Ye, Xi Zhang, Tianbao Xie, Zesen Cheng,
558 Hang Zhang, Zhibo Yang, Haiyang Xu, and Junyang Lin. Qwen2.5-vl technical report, 2025.
559 URL <https://arxiv.org/abs/2502.13923>.
- 560 Camiel J Beukeboom, Christian Burgers, Zsolt P Szabó, Slavica Cvejic, Jan-Erik M Lönnqvist, and
561 Kasper Welbers. The negation bias in stereotype maintenance: A replication in five languages.
562 *Journal of Language and Social Psychology*, 39(2):219–236, 2020.
- 563 Franziska Boenisch, Kamil Deja, Adam Dziedzic, et al. Precise parameter localization for textual
564 generation in diffusion models. *arXiv preprint arXiv:2502.09935*, 2025.
- 565
566 Daniel Bolya, Cheng-Yang Fu, Xiaoliang Dai, Peizhao Zhang, Christoph Feichtenhofer, and Judy
567 Hoffman. Token merging: Your vit but faster. *arXiv preprint arXiv:2210.09461*, 2022.
- 568 Rui Bu, Haofeng Zhong, Wenzheng Chen, and Yangyan Li. Value-state gated attention for mitigating
569 extreme-token phenomena in transformers. *arXiv preprint arXiv:2510.09017*, 2025.
- 570
571 Mu Cai, Haotian Liu, Siva Karthik Mustikovela, Gregory P. Meyer, Yuning Chai, Dennis Park, and
572 Yong Jae Lee. Making large multimodal models understand arbitrary visual prompts. In *IEEE*
573 *Conference on Computer Vision and Pattern Recognition*, 2024.
- 574 Declan Campbell, Sunayana Rane, Tyler Giallanza, Camillo Nicolò De Sabbata, Kia Ghods, Amogh
575 Joshi, Alexander Ku, Steven Frankland, Tom Griffiths, Jonathan D Cohen, et al. Understanding
576 the limits of vision language models through the lens of the binding problem. *Advances in Neural*
577 *Information Processing Systems*, 37:113436–113460, 2024.
- 578
579 Xiaojun Chang, Pengzhen Ren, Pengfei Xu, Zhihui Li, Xiaojiang Chen, and Alex Hauptmann. A
580 comprehensive survey of scene graphs: Generation and application. *IEEE Transactions on Pattern*
581 *Analysis and Machine Intelligence*, 45(1):1–26, 2021.
- 582
583 Chongyan Chen, Samreen Anjum, and Danna Gurari. Vqa therapy: Exploring answer differences
584 by visually grounding answers. In *Proceedings of the IEEE/CVF International Conference on*
Computer Vision, pp. 15315–15325, 2023.
- 585
586 Mu Chen, Liulei Li, Wenguan Wang, and Yi Yang. Diffvsgg: Diffusion-driven online video scene
587 graph generation. In *Proceedings of the Computer Vision and Pattern Recognition Conference*,
588 pp. 29161–29172, 2025a.
- 589
590 Shoufa Chen, Chongjian Ge, Zhan Tong, Jiangliu Wang, Yibing Song, Jue Wang, and Ping Luo.
591 Adaptformer: Adapting vision transformers for scalable visual recognition. *Advances in Neural*
Information Processing Systems, 35:16664–16678, 2022.
- 592
593 Wenxiang Chen, Wei He, Zhiheng Xi, Honglin Guo, Boyang Hong, Jiazheng Zhang, Nijun Li, Tao
Gui, Yun Li, Qi Zhang, et al. Better process supervision with bi-directional rewarding signals. In
Findings of the Association for Computational Linguistics: ACL 2025, pp. 14471–14485, 2025b.

- 594 Xi Chen, Aske Plaat, and Niki van Stein. How does chain of thought think? mechanistic
595 interpretability of chain-of-thought reasoning with sparse autoencoding. *arXiv preprint*
596 *arXiv:2507.22928*, 2025c.
- 597
- 598 Ziyang Chen, Erxue Min, Xiang Zhao, Yunxin Li, Xin Jia, Jinzhi Liao, Jichao Li, Shuaiqiang
599 Wang, Baotian Hu, and Dawei Yin. A question answering dataset for temporal-sensitive retrieval-
600 augmented generation. *Scientific Data*, 12(1):1855, 2025d. ISSN 2052-4463. doi: 10.1038/
601 s41597-025-06098-y. URL <https://doi.org/10.1038/s41597-025-06098-y>.
- 602 Gheorghe Comanici, Eric Bieber, Mike Schaekermann, Ice Pasupat, Noveen Sachdeva, Inderjit
603 Dhillon, Marcel Blistein, Ori Ram, Dan Zhang, Evan Rosen, et al. Gemini 2.5: Pushing the
604 frontier with advanced reasoning, multimodality, long context, and next generation agentic capa-
605 bilities. *arXiv preprint arXiv:2507.06261*, 2025.
- 606
- 607 Ming Dai, Jian Li, Jiedong Zhuang, Xian Zhang, and Wankou Yang. Multi-task visual grounding
608 with coarse-to-fine consistency constraints. In *Proceedings of the AAAI Conference on Artificial*
609 *Intelligence*, volume 39, pp. 2618–2626, 2025.
- 610 Ronghao Dang, Jiangyan Feng, Haodong Zhang, Chongjian Ge, Lin Song, Lijun Gong, Chengju
611 Liu, Qijun Chen, Feng Zhu, Rui Zhao, et al. Instructdet: Diversifying referring object detection
612 with generalized instructions. *arXiv preprint arXiv:2310.05136*, 2023.
- 613
- 614 Erik Daxberger, Nina Wenzel, David Griffiths, Haiming Gang, Justin Lazarow, Gefen Kohavi, Kai
615 Kang, Marcin Eichner, Yinfei Yang, Afshin Dehghan, et al. Mm-spatial: Exploring 3d spatial
616 understanding in multimodal llms. In *Proceedings of the IEEE/CVF International Conference on*
617 *Computer Vision*, pp. 7395–7408, 2025.
- 618 Jiajun Deng, Zhengyuan Yang, Tianlang Chen, Wengang Zhou, and Houqiang Li. Transvg: End-to-
619 end visual grounding with transformers. In *Proceedings of the IEEE/CVF international confer-*
620 *ence on computer vision*, pp. 1769–1779, 2021.
- 621
- 622 Jacob Devlin, Ming-Wei Chang, Kenton Lee, and Kristina Toutanova. Bert: Pre-training of deep
623 bidirectional transformers for language understanding. In *Proceedings of the 2019 conference of*
624 *the North American chapter of the association for computational linguistics: human language*
625 *technologies, volume 1 (long and short papers)*, pp. 4171–4186, 2019.
- 626 Alexey Dosovitskiy, Lucas Beyer, Alexander Kolesnikov, Dirk Weissenborn, Xiaohua Zhai, Thomas
627 Unterthiner, Mostafa Dehghani, Matthias Minderer, Georg Heigold, Sylvain Gelly, et al. An
628 image is worth 16x16 words: Transformers for image recognition at scale. *arXiv preprint*
629 *arXiv:2010.11929*, 2020.
- 630
- 631 Zi-Yi Dou, Aishwarya Kamath, Zhe Gan, Pengchuan Zhang, Jianfeng Wang, Linjie Li, Zicheng Liu,
632 Ce Liu, Yann LeCun, Nanyun Peng, et al. Coarse-to-fine vision-language pre-training with fusion
633 in the backbone. *Advances in neural information processing systems*, 35:32942–32956, 2022.
- 634 Mengnan Du, Fengxiang He, Na Zou, Dacheng Tao, and Xia Hu. Shortcut learning of large language
635 models in natural language understanding. *Communications of the ACM*, 67(1):110–120, 2023.
- 636
- 637 Yuxin Fang, Quan Sun, Xinggang Wang, Tiejun Huang, Xinlong Wang, and Yue Cao. Eva-02: A
638 visual representation for neon genesis. *Image and Vision Computing*, 149:105171, 2024.
- 639
- 640 Shaoxiong Feng, Xuancheng Ren, Kan Li, and Xu Sun. Hierarchical inductive transfer for continual
641 dialogue learning. In Smaranda Muresan, Preslav Nakov, and Aline Villavicencio (eds.), *Findings*
642 *of the Association for Computational Linguistics: ACL 2022*, pp. 693–699, Dublin, Ireland, May
643 2022. Association for Computational Linguistics. doi: 10.18653/v1/2022.findings-acl.57. URL
644 <https://aclanthology.org/2022.findings-acl.57/>.
- 645 Arduin Findeis, Floris Weers, Guoli Yin, Ke Ye, Ruoming Pang, and Tom Gunter. Can external
646 validation tools improve annotation quality for llm-as-a-judge? In *Proceedings of the 63rd Annual*
647 *Meeting of the Association for Computational Linguistics (Volume 1: Long Papers)*, pp. 15997–
16020, 2025.

- 648 Zhizhang FU, Guangsheng Bao, Hongbo Zhang, Chenkai Hu, and Yue Zhang. Correlation or
649 causation: Analyzing the causal structures of llm and lrm reasoning process. *arXiv preprint*
650 *arXiv:2509.17380*, 2025.
- 651
- 652 Chongyang Gao, Kezhen Chen, Jinneng Rao, Baochen Sun, Ruibo Liu, Daiyi Peng, Yawen Zhang,
653 Xiaoyuan Guo, Jie Yang, and VS Subrahmanian. Higher layers need more lora experts. *arXiv*
654 *preprint arXiv:2402.08562*, 2024.
- 655 Chongyang Gao, Kezhen Chen, Jinneng Rao, Ruibo Liu, Baochen Sun, Yawen Zhang, Daiyi Peng,
656 Xiaoyuan Guo, and Vs Subrahmanian. MoLA: MoE LoRA with layer-wise expert allocation. In
657 Luis Chiruzzo, Alan Ritter, and Lu Wang (eds.), *Findings of the Association for Computational*
658 *Linguistics: NAACL 2025*, pp. 5097–5112, Albuquerque, New Mexico, April 2025. Association
659 for Computational Linguistics. ISBN 979-8-89176-195-7. URL [https://aclanthology.](https://aclanthology.org/2025.findings-naacl.284/)
660 [org/2025.findings-naacl.284/](https://aclanthology.org/2025.findings-naacl.284/).
- 661 Walter Gerych, Haoran Zhang, Kimia Hamidieh, Eileen Pan, Maanas K Sharma, Tom Hartvigsen,
662 and Marzyeh Ghassemi. Bendvln: Test-time debiasing of vision-language embeddings. *Advances*
663 *in Neural Information Processing Systems*, 37:62480–62502, 2024.
- 664
- 665 Golnaz Ghiasi, Yin Cui, Aravind Srinivas, Rui Qian, Tsung-Yi Lin, Ekin D Cubuk, Quoc V Le, and
666 Barret Zoph. Simple copy-paste is a strong data augmentation method for instance segmentation.
667 In *Proceedings of the IEEE/CVF conference on computer vision and pattern recognition*, pp.
668 2918–2928, 2021.
- 669 Yongbin Guo, Shuzhen Li, Zhulin Liu, Tong Zhang, and C.L.Philip Chen. A parameter-efficient and
670 fine-grained prompt learning for vision-language models. In Wanxiang Che, Joyce Nabende, Eka-
671 terina Shutova, and Mohammad Taher Pilehvar (eds.), *Proceedings of the 63rd Annual Meeting*
672 *of the Association for Computational Linguistics (Volume 1: Long Papers)*, pp. 31346–31359,
673 Vienna, Austria, July 2025. Association for Computational Linguistics. ISBN 979-8-89176-
674 251-0. doi: 10.18653/v1/2025.acl-long.1514. URL [https://aclanthology.org/2025.](https://aclanthology.org/2025.acl-long.1514/)
675 [acl-long.1514/](https://aclanthology.org/2025.acl-long.1514/).
- 676 Songhao Han, Wei Huang, Hairong Shi, Le Zhuo, Xiu Su, Shifeng Zhang, Xu Zhou, Xiaojuan Qi,
677 Yue Liao, and Si Liu. Videospresso: A large-scale chain-of-thought dataset for fine-grained
678 video reasoning via core frame selection. In *Proceedings of the Computer Vision and Pattern*
679 *Recognition Conference*, pp. 26181–26191, 2025.
- 680
- 681 Zeyu Han, Chao Gao, Jinyang Liu, Jeff Zhang, and Sai Qian Zhang. Parameter-efficient fine-tuning
682 for large models: A comprehensive survey. *arXiv preprint arXiv:2403.14608*, 2024.
- 683 Michael Hanna, Mateusz Piotrowski, Jack Lindsey, and Emmanuel Ameisen. Circuit-tracer: A
684 new library for finding feature circuits. In Yonatan Belinkov, Aaron Mueller, Najoung Kim, Ho-
685 seini Mohebbi, Hanjie Chen, Dana Arad, and Gabriele Sarti (eds.), *Proceedings of the 8th Black-*
686 *boxNLP Workshop: Analyzing and Interpreting Neural Networks for NLP*, pp. 239–249, Suzhou,
687 China, November 2025. Association for Computational Linguistics. ISBN 979-8-89176-346-
688 3. doi: 10.18653/v1/2025.blackboxnlp-1.14. URL [https://aclanthology.org/2025.](https://aclanthology.org/2025.blackboxnlp-1.14/)
689 [blackboxnlp-1.14/](https://aclanthology.org/2025.blackboxnlp-1.14/).
- 690 Amir Hertz, Ron Mokady, Jay Tenenbaum, Kfir Aberman, Yael Pritch, and Daniel Cohen-Or.
691 Prompt-to-prompt image editing with cross attention control. *arXiv preprint arXiv:2208.01626*,
692 2022.
- 693
- 694 Md Mosharaf Hossain, Dhivya Chinnappa, and Eduardo Blanco. An analysis of negation in natural
695 language understanding corpora. *arXiv preprint arXiv:2203.08929*, 2022.
- 696
- 697 Edward J Hu, Yelong Shen, Phillip Wallis, Zeyuan Allen-Zhu, Yanzhi Li, Shean Wang, Lu Wang,
698 Weizhu Chen, et al. Lora: Low-rank adaptation of large language models. *ICLR*, 1(2):3, 2022.
- 699 Taihang Hu, Linxuan Li, Joost van de Weijer, Hongcheng Gao, Fahad Shahbaz Khan, Jian Yang,
700 Ming-Ming Cheng, Kai Wang, and Yaxing Wang. Token merging for training-free semantic
701 binding in text-to-image synthesis. *Advances in Neural Information Processing Systems*, 37:
137646–137672, 2024.

- 702 Aaron Hurst, Adam Lerer, Adam P Goucher, Adam Perelman, Aditya Ramesh, Aidan Clark, AJ Os-
703 trow, Akila Welihinda, Alan Hayes, Alec Radford, et al. Gpt-4o system card. *arXiv preprint*
704 *arXiv:2410.21276*, 2024.
- 705
- 706 Amirmohammad Izadi, Mohammad Ali Banayeeanzade, Fatemeh Askari, Ali Rahimiakbar, Mo-
707 hammad Mahdi Vahedi, Hosein Hasani, and Mahdih Soleymani Baghshah. Visual struc-
708 tures helps visual reasoning: Addressing the binding problem in vlms. *arXiv preprint*
709 *arXiv:2506.22146*, 2025.
- 710 Zeyu Jia, Alexander Rakhlin, and Tengyang Xie. Do we need to verify step by step? rethinking
711 process supervision from a theoretical perspective. *arXiv preprint arXiv:2502.10581*, 2025.
- 712
- 713 Aishwarya Kamath, Mannat Singh, Yann LeCun, Gabriel Synnaeve, Ishan Misra, and Nicolas Car-
714 ion. Mdetr-modulated detection for end-to-end multi-modal understanding. In *Proceedings of the*
715 *IEEE/CVF international conference on computer vision*, pp. 1780–1790, 2021.
- 716
- 717 Evangelos Kazakos, Cordelia Schmid, and Josef Sivic. Large-scale pre-training for grounded video
718 caption generation. *arXiv preprint arXiv:2503.10781*, 2025.
- 719
- 720 Fucui Ke, Joy Hsu, Zhixi Cai, Zixian Ma, Xin Zheng, Xindi Wu, Sukai Huang, Weiqing Wang,
721 Pari Delir Haghighi, Gholamreza Haffari, et al. Explain before you answer: A survey on compo-
722 sitional visual reasoning. *arXiv preprint arXiv:2508.17298*, 2025.
- 723
- 724 Dahun Kim, Anelia Angelova, and Weicheng Kuo. Region-aware pretraining for open-vocabulary
725 object detection with vision transformers. In *Proceedings of the IEEE/CVF conference on com-
726 puter vision and pattern recognition*, pp. 11144–11154, 2023a.
- 727
- 728 Dahun Kim, AJ Piergiovanni, Ganesh Mallya, and Anelia Angelova. Videocomp: Advancing fine-
729 grained compositional and temporal alignment in video-text models. In *Proceedings of the Com-
730 puter Vision and Pattern Recognition Conference*, pp. 29060–29070, 2025.
- 731
- 732 Yeongbin Kim, Gautam Singh, Junyeong Park, Caglar Gulcehre, and Sungjin Ahn. Imagine the
733 unseen world: a benchmark for systematic generalization in visual world models. *Advances in*
734 *Neural Information Processing Systems*, 36:27880–27896, 2023b.
- 735
- 736 Jian Lan, Yifei Fu, Udo Schlegel, Gengyuan Zhang, Tanveer Hannan, Haokun Chen, and Thomas
737 Seidl. My answer is not ‘fair’: Mitigating social bias in vision-language models via fair and biased
738 residuals. *arXiv preprint arXiv:2505.23798*, 2025.
- 739
- 740 Hugo Laurençon, Léo Tronchon, Matthieu Cord, and Victor Sanh. What matters when building
741 vision-language models? *Advances in Neural Information Processing Systems*, 37:87874–87907,
742 2024.
- 743
- 744 Nicholas Lee, Thanakul Wattanawong, Sehoon Kim, Karttikeya Mangalam, Sheng Shen, Gopala
745 Anumanchipalli, Michael Mahoney, Kurt Keutzer, and Amir Gholami. Llm2llm: Boosting llms
746 with novel iterative data enhancement. In *Findings of the Association for Computational Linguis-
747 tics: ACL 2024*, pp. 6498–6526, 2024.
- 748
- 749 Alexander Cong Li, Ananya Kumar, and Deepak Pathak. Generative classifiers avoid shortcut
750 solutions. In *International Conference on Learning Representations (ICLR)*, 2025a. URL
751 <https://openreview.net/pdf?id=oCUYc7BzXQ>. Poster Presentation.
- 752
- 753 Chuanhao Li, Chenchen Jing, Zhen Li, Mingliang Zhai, Yuwei Wu, and Yunde Jia. In-context
754 compositional generalization for large vision-language models. In Yaser Al-Onaizan, Mohit
755 Bansal, and Yun-Nung Chen (eds.), *Proceedings of the 2024 Conference on Empirical Meth-
ods in Natural Language Processing*, pp. 17954–17966, Miami, Florida, USA, November 2024a.
Association for Computational Linguistics. doi: 10.18653/v1/2024.emnlp-main.996. URL
<https://aclanthology.org/2024.emnlp-main.996/>.
- 756
- 757 Chuanhao Li, Wenbo Ye, Zhen Li, Yuwei Wu, and Yunde Jia. Multi-sourced compositional gener-
758 alization in visual question answering. *arXiv preprint arXiv:2505.23045*, 2025b.

- 756 Liunian Li, Zi-Yi Dou, Nanyun Peng, and Kai-Wei Chang. Desco: Learning object recognition
757 with rich language descriptions. *Advances in Neural Information Processing Systems*, 36:37511–
758 37526, 2023.
- 759
760 Liunian Harold Li, Pengchuan Zhang, Haotian Zhang, Jianwei Yang, Chunyuan Li, Yiwu Zhong,
761 Lijuan Wang, Lu Yuan, Lei Zhang, Jenq-Neng Hwang, et al. Grounded language-image pre-
762 training. In *Proceedings of the IEEE/CVF conference on computer vision and pattern recognition*,
763 pp. 10965–10975, 2022.
- 764 Tianle Li, Jihai Zhang, Yongming Rao, and Yu Cheng. Unveiling the compositional ability gap in
765 vision-language reasoning model. *arXiv preprint arXiv:2505.19406*, 2025c.
- 766
767 Wentong Li, Yuqian Yuan, Jian Liu, Dongqi Tang, Song Wang, Jie Qin, Jianke Zhu, and Lei Zhang.
768 Tokenpacker: Efficient visual projector for multimodal llm. *arXiv preprint arXiv:2407.02392*,
769 2024b.
- 770
771 Yanjun Li, Zhaoyang Li, Honghui Chen, and Lizhi Xu. Unbiased video scene graph generation
772 via visual and semantic dual debiasing. In *Proceedings of the Computer Vision and Pattern
773 Recognition Conference*, pp. 19047–19056, 2025d.
- 774
775 Hunter Lightman, Vineet Kosaraju, Yuri Burda, Harrison Edwards, Bowen Baker, Teddy Lee, Jan
776 Leike, John Schulman, Ilya Sutskever, and Karl Cobbe. Let’s verify step by step. In *The Twelfth
777 International Conference on Learning Representations*, 2023.
- 778
779 Ziyi Lin, Chris Liu, Renrui Zhang, Peng Gao, Longtian Qiu, Han Xiao, Han Qiu, Chen Lin, Wenqi
780 Shao, Keqin Chen, et al. Sphinx: The joint mixing of weights, tasks, and visual embeddings for
781 multi-modal large language models. *arXiv preprint arXiv:2311.07575*, 2023.
- 782
783 Shih-Yang Liu, Chien-Yi Wang, Hongxu Yin, Pavlo Molchanov, Yu-Chiang Frank Wang, Kwang-
784 Ting Cheng, and Min-Hung Chen. Dora: Weight-decomposed low-rank adaptation. In *Forty-first
785 International Conference on Machine Learning*, 2024a.
- 786
787 Shilong Liu, Zhaoyang Zeng, Tianhe Ren, Feng Li, Hao Zhang, Jie Yang, Qing Jiang, Chunyuan
788 Li, Jianwei Yang, Hang Su, et al. Grounding dino: Marrying dino with grounded pre-training
789 for open-set object detection. In *European Conference on Computer Vision*, pp. 38–55. Springer,
790 2024b.
- 791
792 Ze Liu, Yutong Lin, Yue Cao, Han Hu, Yixuan Wei, Zheng Zhang, Stephen Lin, and Baining Guo.
793 Swin transformer: Hierarchical vision transformer using shifted windows. In *Proceedings of the
794 IEEE/CVF international conference on computer vision*, pp. 10012–10022, 2021.
- 795
796 Ilya Loshchilov and Frank Hutter. Decoupled weight decay regularization. *arXiv preprint
797 arXiv:1711.05101*, 2017.
- 798
799 Roser Morante and Eduardo Blanco. Recent advances in processing negation. *Natural Language
800 Engineering*, 27(2):121–130, 2021.
- 801
802 Roser Morante and Walter Daelemans. Conandoyle-neg: Annotation of negation in conan doyle sto-
803 ries. In *Proceedings of the eighth international conference on language resources and evaluation,
804 istanbul*, pp. 1563–1568. Citeseer, 2012.
- 805
806 Roser Morante and Caroline Sporleder. Modality and negation: An introduction to the special issue.
807 *Computational linguistics*, 38(2):223–260, 2012.
- 808
809 Aashiq Muhamed, Mona Diab, and Virginia Smith. Decoding dark matter: Specialized sparse au-
810 toencoders for interpreting rare concepts in foundation models. In *Findings of the Association for
811 Computational Linguistics: NAACL 2025*, pp. 1604–1635, 2025.
- 812
813 Nilay Naharas, Dang Nguyen, Nesihan Bulut, Mohammadhossein Bateni, Vahab Mirrokni, and
814 Baharan Mirzasoleiman. Data selection for fine-tuning vision language models via cross modal
815 alignment trajectories. *arXiv preprint arXiv:2510.01454*, 2025.

- 810 Narges Norouzi, Svetlana Orlova, Daan De Geus, and Gijs Dubbelman. Algm: Adaptive local-
811 then-global token merging for efficient semantic segmentation with plain vision transformers.
812 In *Proceedings of the IEEE/CVF Conference on Computer Vision and Pattern Recognition*, pp.
813 15773–15782, 2024.
- 814 Bo Pang, Tingrui Qiao, Caroline Walker, Chris Cunningham, and Yun Sing Koh. Cabin: Debiasing
815 vision-language models using backdoor adjustments. In James Kwok (ed.), *Proceedings of the*
816 *Thirty-Fourth International Joint Conference on Artificial Intelligence, IJCAI-25*, pp. 484–492.
817 International Joint Conferences on Artificial Intelligence Organization, 8 2025. doi: 10.24963/
818 ijcai.2025/55. URL <https://doi.org/10.24963/ijcai.2025/55>. Main Track.
- 819 Junsung Park, Jungbeom Lee, Jongyoon Song, Sangwon Yu, Dahuin Jung, and Sungroh Yoon.
820 Know” no” better: A data-driven approach for enhancing negation awareness in clip. *arXiv*
821 *preprint arXiv:2501.10913*, 2025.
- 822 Junyoung Park, Jin Kim, Hyeongjun Kwon, Ilhoon Yoon, and Kwanghoon Sohn. Layer-wise auto-
823 weighting for non-stationary test-time adaptation. In *Proceedings of the IEEE/CVF Winter Con-*
824 *ference on Applications of Computer Vision*, pp. 1414–1423, 2024a.
- 825 Kwanyong Park, Kuniaki Saito, and Donghyun Kim. Weak-to-strong compositional learning from
826 generative models for language-based object detection. In *European Conference on Computer*
827 *Vision*, pp. 1–19. Springer, 2024b.
- 828 Trong Thang Pham, Ngoc-Vuong Ho, Nhat-Tan Bui, Thinh Phan, Patel Brijesh, Donald Adjeroh,
829 Gianfranco Doretto, Anh Nguyen, Carol C Wu, Hien Nguyen, et al. Fg-cxr: a radiologist-aligned
830 gaze dataset for enhancing interpretability in chest x-ray report generation. In *Proceedings of the*
831 *Asian conference on computer vision*, pp. 941–958, 2024.
- 832 Bryan A Plummer, Liwei Wang, Chris M Cervantes, Juan C Caicedo, Julia Hockenmaier, and Svet-
833 lana Lazebnik. Flickr30k entities: Collecting region-to-phrase correspondences for richer image-
834 to-sentence models. In *Proceedings of the IEEE international conference on computer vision*, pp.
835 2641–2649, 2015.
- 836 Daniel Reich and Tanja Schultz. Uncovering the full potential of visual grounding methods in VQA.
837 In Lun-Wei Ku, Andre Martins, and Vivek Srikumar (eds.), *Proceedings of the 62nd Annual Meet-*
838 *ing of the Association for Computational Linguistics (Volume 1: Long Papers)*, pp. 4406–4419,
839 Bangkok, Thailand, August 2024. Association for Computational Linguistics. doi: 10.18653/v1/
840 2024.acl-long.241. URL <https://aclanthology.org/2024.acl-long.241/>.
- 841 Zahra Sarabi and Eduardo Blanco. Understanding negation in positive terms using syntactic de-
842 pendencies. In *Proceedings of the 2016 Conference on Empirical Methods in Natural Language*
843 *Processing*, pp. 1108–1118, 2016.
- 844 Christoph Schuhmann, Richard Vencu, Romain Beaumont, Robert Kaczmarczyk, Clayton Mullis,
845 Aarush Katta, Theo Coombes, Jenia Jitsev, and Aran Komatsuzaki. Laion-400m: Open dataset of
846 clip-filtered 400 million image-text pairs. *arXiv preprint arXiv:2111.02114*, 2021.
- 847 Samuel Schuster, Vijay Kumar B G, Yumin Suh, Konstantinos M. Dafnis, Zhixing Zhang, Shiyu
848 Zhao, and Dimitris Metaxas. Omnilabel: A challenging benchmark for language-based object
849 detection. In *ICCV*, 2023.
- 850 Dominykas Seputis, Serghei Mihailov, Soham Chatterjee, and Zehao Xiao. Multi-modal adapter for
851 vision-language models. *arXiv preprint arXiv:2409.02958*, 2024.
- 852 Ashish Seth, Mayur Hemani, and Chirag Agarwal. Dear: Debiasing vision-language models with
853 additive residuals. In *Proceedings of the IEEE/CVF Conference on Computer Vision and Pattern*
854 *Recognition*, pp. 6820–6829, 2023.
- 855 Yunhang Shen, Chaoyou Fu, Peixian Chen, Mengdan Zhang, Ke Li, Xing Sun, Yunsheng Wu,
856 Shaohui Lin, and Rongrong Ji. Aligning and prompting everything all at once for universal
857 visual perception. In *Proceedings of the IEEE/CVF Conference on Computer Vision and Pattern*
858 *Recognition*, pp. 13193–13203, 2024.

- 864 Robik Shrestha, Kushal Kafle, and Christopher Kanan. A negative case analysis of visual ground-
865 ing methods for VQA. In Dan Jurafsky, Joyce Chai, Natalie Schluter, and Joel Tetreault (eds.),
866 *Proceedings of the 58th Annual Meeting of the Association for Computational Linguistics*, pp.
867 8172–8181, Online, July 2020a. Association for Computational Linguistics. doi: 10.18653/v1/
868 2020.acl-main.727. URL <https://aclanthology.org/2020.acl-main.727/>.
- 869 Robik Shrestha, Kushal Kafle, and Christopher Kanan. Visual grounding methods for vqa are work-
870 ing for the wrong reasons! *arXiv preprint arXiv:2004.05704*, 2020b.
- 872 Richard Socher, Alex Perelygin, Jean Wu, Jason Chuang, Christopher D. Manning, Andrew Ng, and
873 Christopher Potts. Recursive deep models for semantic compositionality over a sentiment tree-
874 bank. In David Yarowsky, Timothy Baldwin, Anna Korhonen, Karen Livescu, and Steven Bethard
875 (eds.), *Proceedings of the 2013 Conference on Empirical Methods in Natural Language Process-*
876 *ing*, pp. 1631–1642, Seattle, Washington, USA, October 2013. Association for Computational
877 Linguistics. URL <https://aclanthology.org/D13-1170/>.
- 878 Jiajun Song, Zhuoyan Xu, and Yiqiao Zhong. Out-of-distribution generalization via composition: a
879 lens through induction heads in transformers. *Proceedings of the National Academy of Sciences*,
880 122(6):e2417182122, 2025.
- 882 Wei Su, Peihan Miao, Huanzhang Dou, and Xi Li. Scanformer: Referring expression comprehension
883 by iteratively scanning. In *Proceedings of the IEEE/CVF Conference on Computer Vision and*
884 *Pattern Recognition*, pp. 13449–13458, 2024.
- 885 Quan Sun, Yuxin Fang, Ledell Wu, Xinlong Wang, and Yue Cao. Eva-clip: Improved training
886 techniques for clip at scale. *arXiv preprint arXiv:2303.15389*, 2023.
- 888 György Szarvas, Veronika Vincze, Richárd Farkas, and János Csirik. The bioscope corpus: annota-
889 tion for negation, uncertainty and their scope in biomedical texts. In *Proceedings of the workshop*
890 *on current trends in biomedical natural language processing*, pp. 38–45, 2008.
- 892 Alon Talmor, Jonathan Herzig, Nicholas Lourie, and Jonathan Berant. Commonsenseqa: A question
893 answering challenge targeting commonsense knowledge. In *Proceedings of the 2019 Conference*
894 *of the North American Chapter of the Association for Computational Linguistics: Human Lan-*
895 *guage Technologies, Volume 1 (Long and Short Papers)*, pp. 4149–4158, 2019.
- 896 Zhen Tan, Dawei Li, Song Wang, Alimohammad Beigi, Bohan Jiang, Amrita Bhattacharjee, Man-
897 sooreh Karami, Jundong Li, Lu Cheng, and Huan Liu. Large language models for data annotation
898 and synthesis: A survey. *arXiv preprint arXiv:2402.13446*, 2024.
- 899 Jean-Francois Ton, Muhammad Faaiz Taufiq, and Yang Liu. Understanding chain-of-thought in llms
900 through information theory. *arXiv preprint arXiv:2411.11984*, 2024.
- 902 David Wan, Jaemin Cho, Elias Stengel-Eskin, and Mohit Bansal. Contrastive region guidance:
903 Improving grounding in vision-language models without training. In *European Conference on*
904 *Computer Vision*, pp. 198–215. Springer, 2024.
- 905 Shijie Wang, Dahun Kim, Ali Taalimi, Chen Sun, and Weicheng Kuo. Learning visual grounding
906 from generative vision and language model. In *2025 IEEE/CVF Winter Conference on Applica-*
907 *tions of Computer Vision (WACV)*, pp. 8057–8067. IEEE, 2025a.
- 908 Yudong Wang, Zixuan Fu, Jie Cai, Peijun Tang, Hongya Lyu, Yewei Fang, Zhi Zheng, Jie Zhou,
909 Guoyang Zeng, Chaojun Xiao, et al. Ultra-fineweb: Efficient data filtering and verification for
910 high-quality llm training data. *arXiv preprint arXiv:2505.05427*, 2025b.
- 912 Linhui Xiao, Xiaoshan Yang, Xiangyuan Lan, Yaowei Wang, and Changsheng Xu. Towards visual
913 grounding: A survey. *arXiv preprint arXiv:2412.20206*, 2024.
- 914 Teng Xiao, Zhen Ge, Sujay Sanghavi, Tian Wang, Julian Katz-Samuels, Marc Versage, Qingjun
915 Cui, and Trishul Chilimbi. InfoPO: On mutual information maximization for large language
916 model alignment. In Luis Chiruzzo, Alan Ritter, and Lu Wang (eds.), *Proceedings of the 2025*
917 *Conference of the Nations of the Americas Chapter of the Association for Computational Linguis-*
tics: Human Language Technologies (Volume 1: Long Papers), pp. 11699–11711, Albuquerque,

- 918 New Mexico, April 2025. Association for Computational Linguistics. ISBN 979-8-89176-189-
919 6. doi: 10.18653/v1/2025.naacl-long.585. URL <https://aclanthology.org/2025.naacl-long.585/>.
- 921
922 Chi Xie, Zhao Zhang, Yixuan Wu, Feng Zhu, Rui Zhao, and Shuang Liang. Described object
923 detection: Liberating object detection with flexible expressions. *Advances in Neural Information
924 Processing Systems*, 36:79095–79107, 2023.
- 925 Huihui Xu, Jiashi Lin, Haoyu Chen, Junjun He, and Lei Zhu. Eventrr: Event referential reasoning
926 for referring video object segmentation. *arXiv preprint arXiv:2508.07171*, 2025.
- 927
928 Yi Yang, Hanyu Duan, Ahmed Abbasi, John P. Lalor, and Kar Yan Tam. Bias a-head? analyzing
929 bias in transformer-based language model attention heads. In Trista Cao, Anubrata Das, Tharindu
930 Kumara, Yixin Wan, Satyapriya Krishna, Ninareh Mehrabi, Jwala Dhamala, Anil Ramakrishna,
931 Aram Galystan, Anoop Kumar, Rahul Gupta, and Kai-Wei Chang (eds.), *Proceedings of the 5th
932 Workshop on Trustworthy NLP (TrustNLP 2025)*, pp. 276–290, Albuquerque, New Mexico, May
933 2025. Association for Computational Linguistics. ISBN 979-8-89176-233-6. doi: 10.18653/v1/
934 2025.trustnlp-main.18. URL <https://aclanthology.org/2025.trustnlp-main.18/>.
- 935
936 Yu Yang, Eric Gan, Gintare Karolina Dziugaite, and Baharan Mirzasoleiman. Identifying spurious
937 biases early in training through the lens of simplicity bias. In *International conference on artificial
938 intelligence and statistics*, pp. 2953–2961. PMLR, 2024.
- 939
940 Lewei Yao, Jianhua Han, Youpeng Wen, Xiaodan Liang, Dan Xu, Wei Zhang, Zhenguo Li, Chunjing
941 Xu, and Hang Xu. Detclip: Dictionary-enriched visual-concept paralleled pre-training for open-
942 world detection. *Advances in Neural Information Processing Systems*, 35:9125–9138, 2022.
- 943
944 Yiyang Yao, Peng Liu, Tiancheng Zhao, Qianqian Zhang, Jiajia Liao, Chunxin Fang, Kyusong Lee,
945 and Qing Wang. How to evaluate the generalization of detection? a benchmark for comprehensive
946 open-vocabulary detection. In *Proceedings of the AAAI Conference on Artificial Intelligence*,
947 volume 38, pp. 6630–6638, 2024.
- 948
949 Maxime Zanella and Ismail Ben Ayed. Low-rank few-shot adaptation of vision-language models.
950 In *Proceedings of the IEEE/CVF Conference on Computer Vision and Pattern Recognition*, pp.
951 1593–1603, 2024.
- 952
953 Alireza Zareian, Kevin Dela Rosa, Derek Hao Hu, and Shih-Fu Chang. Open-vocabulary object
954 detection using captions. In *Proceedings of the IEEE/CVF conference on computer vision and
955 pattern recognition*, pp. 14393–14402, 2021.
- 956
957 Hanzhi Zhang, Heng Fan, Kewei Sha, Yan Huang, and Yunhe Feng. Dam: Dynamic attention mask
958 for long-context large language model inference acceleration. *arXiv preprint arXiv:2506.11104*,
959 2025.
- 960
961 Shiyu Zhao, Long Zhao, Yumin Suh, Dimitris N Metaxas, Manmohan Chandraker, Samuel Schulter,
962 et al. Generating enhanced negatives for training language-based object detectors. In *Proceedings
963 of the IEEE/CVF Conference on Computer Vision and Pattern Recognition*, pp. 13592–13602,
964 2024a.
- 965
966 Tiancheng Zhao, Peng Liu, and Kyusong Lee. Omdet: Large-scale vision-language multi-dataset
967 pre-training with multimodal detection network. *IET Computer Vision*, 18(5):626–639, 2024b.
- 968
969 Zheng Zhao, Yeskendir Koishkenov, Xianjun Yang, Naila Murray, and Nicola Cancedda. Verifying
970 chain-of-thought reasoning via its computational graph. *arXiv preprint arXiv:2510.09312*, 2025.
- 971
972 Guangtao Zheng, Wenqian Ye, and Aidong Zhang. Shortcutprobe: Probing prediction shortcuts for
973 learning robust models. *arXiv preprint arXiv:2505.13910*, 2025.
- 974
975 Xizhou Zhu, Weijie Su, Lewei Lu, Bin Li, Xiaogang Wang, and Jifeng Dai. Deformable detr:
976 Deformable transformers for end-to-end object detection. *arXiv preprint arXiv:2010.04159*, 2020.
- 977
978 Wei Li Zuwei Long. Open grounding dino:the third party implementation of the paper grounding
979 dino. <https://github.com/longzw1997/Open-GroundingDino>, 2023.

SUPPLEMENTARY MATERIALS

We provide supplementary materials in the following order:

- Section **A: COVAND Details** describing our negation-focused dataset construction pipeline, including the three-step Chain-of-Thought prompt design, VQA-based caption alignment, negation cue distribution, and a human-in-the-loop data error analysis.
- Section **B: Implementation Details** of all backbone architectures and our LoRA placement strategy, together with additional attention visualizations.
- Section **C: Extended Related Work** covering CoT-based dataset construction, visual grounding and region-level alignment, parameter-efficient fine-tuning for VLMs, compositional reasoning, and bias mitigation.
- Section **D: Additional Ablations: Negation- and Noun-Only Boosting**, which compare simple token-level boosting and attention-bias variants against our NEGTOME.
- Section **E: Comparison with Post-hoc VQA Methods** analyzing two-stage detector+VQA pipelines and their accuracy–latency trade-offs.
- Section **F: Evaluation on Full OVDEval Subsets** reporting results on all OVDEval subset.
- Section **G: Analysis on RPN-based Detectors** contrasting RPN-based and DETR-style architectures under negation.
- Section **H: Zero-shot Downstream NegBench MCQ** presenting a detailed breakdown of the multiple-choice subsets and characteristic error patterns.
- Section **I: Qualitative Results** displaying additional examples on OVDEval and D³, as well as representative failure cases on complex negation and event-level reasoning.
- Section **J: Declarations** summarizing LLM usage, ethics, and reproducibility.

A DETAILS ON COVAND

A.1 PROMPT FOR THREE-STEP COT CAPTION GENERATION

We employ a systematic three-step CoT reasoning approach using GPT-4o (Hurst et al., 2024) to generate high-quality negation-focused captions. As shown in Figure S11, the prompt structure is carefully designed to elicit temporally coherent reasoning that produces semantically valid negation captions grounded in the visual content.

Our prompt begins by informing the model that it will be provided with an image containing a highlighted bounding box, along with a target phrase describing the main subject in the region. The model is then guided through three distinct reasoning steps:

A.1.1 STEP 1: ATTRIBUTE EXTRACTION

The model first generates two comprehensive lists of attributes:

- **Present Attribute** (A_{pres}): At least three attributes or keyword items clearly visible within the bounded region.
- **Absent Attribute** (A_{abs}): At least three attributes or keyword items that are contextually relevant but clearly not present in the bounded region.

A.1.2 STEP 2: CAPTION GENERATION

Using the attributes from Step 1, the model produces two types of captions:

- **Negative Caption** (C_{neg}): Creates a factually incorrect statement by falsely claiming an existing attribute is absent. This caption must contain a negation expression (e.g., “no”, “not”, “without”) coupled with an attribute from the existing contents list.

- **Positive Caption (C_{pos}):** Creates a factually correct statement by accurately describing an absent attribute as absent. This caption pairs a negation expression with an attribute from the absent contents list.

This approach yields contrastive pairs where the negative caption contradicts the visual evidence while the positive caption aligns with it, creating training data that specifically targets negation understanding.

A.1.3 STEP 3: SEMANTIC VERIFICATION

For quality assurance, each generated caption undergoes verification:

- **Negative Verification:** Confirms the caption (1) contains a negation expression, (2) references an existing attribute from Step 1, and (3) factually mismatches the actual content of the bounded region.
- **Positive Verification:** Confirms the caption (1) contains a negation expression, (2) references an absent attribute from Step 1, and (3) correctly describes the absence of the attribute in a way relevant to the context.

This verification step ensures semantic integrity and prevents generation artifacts by applying explicit logical checks. If either caption fails verification, the process iteratively regenerates captions until valid pairs are produced or the retry limit is reached.

The prompt enforces concise, natural language expressions with a single-sentence structure. As examples in Figure S12 and Figure S13, it requires the model to focus exclusively on the bounded region, preventing semantic drift to other parts of the image. The entire process outputs a structured JSON format containing the attribute lists, caption pairs, and verification rationales, facilitating downstream dataset creation and quality control processes.

A.2 VQA-BASED CAPTION ALIGNMENT

To address a critical challenge in negation-aware detection, ensuring generated captions reference exclusively the intended bounding box rather than other visually similar regions, we implement a structured verification pipeline with VQA alignment.

First, we apply alphabetical region labeling to all bounding boxes that share the target phrase type (e.g., “person”) by assigning distinct markers (A, B, C, ...) to each instance. The originally prompted region remains unlabeled to avoid biasing the verification process. As shown in Figure S14, our visual prompting approach carefully considers label placement to maintain visual clarity. When labeling multiple instances of the same type (e.g., multiple “person” boxes), we position alphabetical markers outside the top-left corner of each bounding box to avoid occluding the object itself. This placement strategy preserves the visual integrity of the object while providing clear reference points for the VQA model. In cases where objects appear near image boundaries, we adaptively place labels inside the top-left corner of the bounding box to ensure they remain visible within the frame. This adaptive positioning is crucial for maintaining consistent label visibility across diverse image compositions.

Then, for each caption pair (C_{pos}, C_{neg}), we query a multimodal VQA model with two precisely formulated questions as in Figure S15. The VQA model analyzes the image and captions to produce structured JSON responses specifying matching box labels. A valid alignment requires that C_{pos} matches *exactly* the original unlabeled region, while C_{neg} either matches no regions (‘None’) or incorrectly matches another box. This process effectively eliminates label noises: false negatives, where C_{neg} accidentally describes another instance, and ambiguous groundings, where captions generically describe multiple regions.

Figure S16 showcases several successful examples from our complete caption generation pipeline. In these examples, we can observe how the three-step CoT process first generates attribute-based negative and positive captions for the target region, followed by the VQA alignment step that verifies caption-region correspondence. Despite the effectiveness of our approach, we encountered certain limitations in complex scenes, as illustrated in Figure S17. When multiple instances of the same type are densely clustered, the visual prompting can become ambiguous, making it difficult for the

VQA model to determine precise correspondences. To maintain dataset quality, we implemented a filtering mechanism that excludes images containing more than five instances of the same type from the caption generation process. This threshold was empirically determined to balance the diversity of the dataset with the precision of the annotation, ensuring that our training data provides unambiguous supervision signals for understanding the meaning of negations.

A.3 DATASET DISTRIBUTION

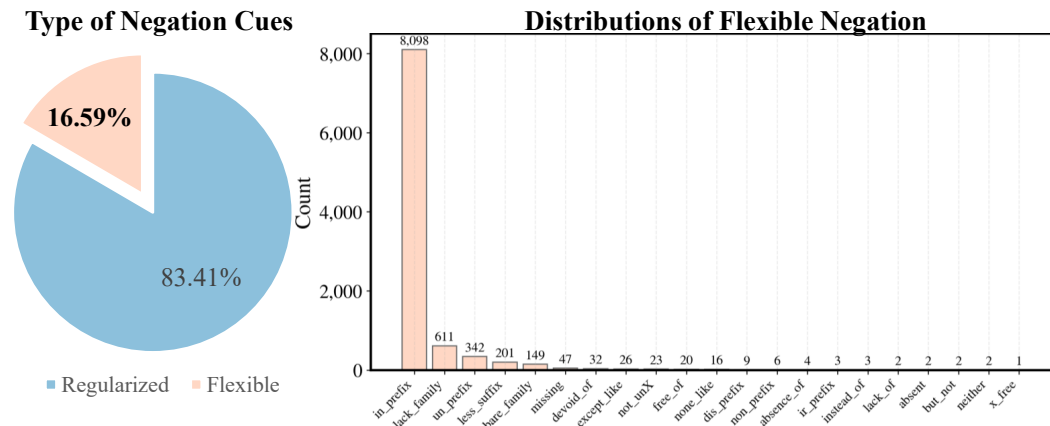


Figure S8: **Distributions of Negation Type.** Analyzing all 48,761 captions in COVAND and identified 57,874 negation instances. Following standard linguistic taxonomies, we categorized them into Regularized (explicit syntactic markers) and Flexible (lexical/morphological) cues. Regularized Cues means high-frequency surface markers, including not, no, without, never, and contractions like n't. Flexible Cues means a diverse long-tail of expressions including lack, un-, in-/im-/ir-, dis-, non-, and -less.

We separate surface **regularized cues** versus **flexible cues** as below:

- **Regularized cues** are short, high-frequency surface markers: not, without, no, never, and clitic contractions n't.
- **Flexible cues** cover lexical and morphological forms that naturally occur in open text: *lack-family* (lack, lacks, lacking, lack of), devoid of, absence of/absent, coordinations (neither/nor, but not, rather than, instead of), and productive morphology such as negative prefixes/suffixes (in-/im-/il-/ir-, un-, dis-, non-), and -less, as well as X-free/free of.

We analyze all 48,761 captions (24,381 *positive* vs. 24,380 *negative*). Across all captions, we detect 57,874 negation cues in total: **48,275 regularized** (83.41%) and **9,599 flexible** (16.59%).

Prior analyses of negation in natural language understanding corpora show that explicit markers such as not, no, and n't account for the large majority of negation instances. Hossain et al. (2022) found that syntactic negation (regularized cues) constitutes 88.6% in CommonsenseQA (Talmor et al., 2019) and 71.9% in SST-2 (Socher et al., 2013), compared to morphological negation (11.4% and 28.1%, respectively) as in (Hossain et al., 2022). While these figures come from specific NLU datasets rather than unrestricted natural language, they suggest that regularized forms are prevalent in realistic language tasks. Thus, our dataset's 83.41% regularized distribution is not solely an artifact of GPT-4o's generation bias, but rather aligns with patterns observed in existing negation-annotated corpora for downstream applications.

Flexible forms provide meaningful diversity. While regularized cues dominate, the presence of 9,599 flexible cues (16.59%) ensures the dataset includes a non-trivial variety of negation expressions. This diversity is essential for evaluating whether models generalize beyond high-frequency patterns. Flexible negations, though less common, are critical in compositional reasoning tasks such as DOD, where attribute-level and relational negations often require nuanced understanding. By

including both regularized and flexible forms, CoVAND provides a more comprehensive training signal than datasets relying solely on template-based augmentation.

Future work: Mitigating prompt bias for richer flexibility. We acknowledge that the current distribution may still reflect prompt-design bias inherent to GPT-4o’s training data. To further enhance the diversity of flexible negation forms, future iterations of CoVAND could employ targeted prompt engineering strategies—such as explicitly requesting diverse negation structures (e.g., “describe the absence using lexical negation such as *lack* or *devoid of*”)—or post-hoc augmentation techniques to rewrite regularized negations into their flexible counterparts. Such refinements could yield a more balanced distribution while preserving the semantic integrity established by our CoT and VQA pipeline.

A.4 DATA ERROR CASE ANALYSIS

To quantify residual annotation errors in CoVAND, we perform a two-stage *human-in-the-loop* audit combining an independent multimodal language model with manual inspection.

Stage 1: Automated cross-model audit. We first randomly sample 1,000 image–caption pairs from the training split of CoVAND. Each sample consists of an image, a target bounding box, and a pair of captions describing the same region: a *negative* caption (hard negative, e.g., “a boy without a helmet”) and a *positive* caption (true description, e.g., “a boy without a backpack”), together with the key attribute mentioned in the caption (“helmet”, “backpack”, *etc.*).

For each sample, we generate a visual prompt by overlaying a red rectangle on the target bounding box and feed the resulting image, the caption, and the attribute to an off-the-shelf multimodal LLM, Gemini-2.5 (Comanici et al., 2025), that is architecturally and training-wise independent from the model used in our data generation pipeline. The model is instructed to act as an objective judge and to return a structured JSON answer indicating whether the attribute is visually *present* in the red box:

```
{
  "is_attribute_present": boolean,
  "reasoning": "short explanation"
}
```

We then apply a deterministic decision rule to compare the dataset label with the model’s prediction:

- For a negative caption (intended hard negative of the form “*X* without *Y*”), the example is considered *valid* if the attribute *Y* is in fact present in the region (`is_attribute_present = true`).
- For a positive caption (intended true caption of the form “*X* without *Y*”), the example is considered *valid* if the attribute *Y* is indeed absent (`is_attribute_present = false`).

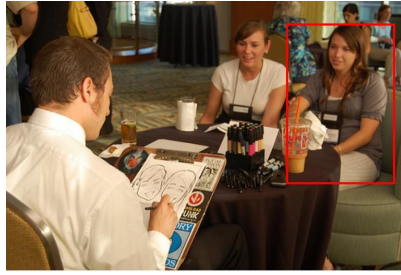
For each caption, we log the full record (image path, bounding box, caption type, attribute, model verdict, and free-form reasoning) in a JSON file for subsequent human analysis.

Over 1,000 sampled pairs, the independent model disagrees with the CoVAND label in 78 cases (7.8%). These disagreements define the pool of potentially erroneous annotations.

Stage 2: Manual verification of disagreements. In the second stage, we load the logged results and focus on the disagreement set. A lightweight visualization tool displays, for each case, the original image with the red bounding box plus textual metadata (caption, attribute, model verdict, and reasoning). Annotators then categorize each disagreement as either:

- **Dataset error:** the CoVAND label is incorrect and the independent model’s judgment is correct, or
- **Model error:** the CoVAND label is correct and the independent model misinterprets the visual evidence.

1188
1189
1190
1191
1192
1193
1194
1195
1196
1197
1198
1199
1200
1201
1202
1203
1204
1205
1206
1207
1208
1209
1210
1211
1212
1213
1214
1215
1216
1217
1218
1219
1220
1221
1222
1223
1224
1225
1226
1227
1228
1229
1230
1231
1232
1233
1234
1235
1236
1237
1238
1239
1240
1241



C_{neg} : "The caricature of young women is *not* holding a drink."
 Gemini does not saw A_{pres} "holding a drink".
 The woman in the red bounding box is not holding a drink. A drink is on the table in front of her, but her hands are resting on the table and in her lap.



C_{neg} : "The jacket is *not* blue."
 Gemini does not saw A_{pres} "blue jacket".
 Person in the bounding box is wearing a yellow life vest over a grey or light-colored jacket.

Figure S9: **Representative dataset errors for negative captions.** Each panel shows an image with the target region highlighted and the corresponding hard-negative caption ("X without Y"). Many mislabels arise in visually subtle cases (e.g. barely visible or skin-colored attributes) where the "absent" attribute Y is in fact present but difficult to perceive even for humans.



C_{pos} : "A male surgeon performs surgery *without* gloves on his hands."
 Gemini saw A_{abs} "gloves".
 The surgeon inside the red bounding box is wearing skin-toned surgical gloves on both of his hands.



C_{pos} : "The helmet does *not* have a camouflage pattern."
 Gemini saw A_{abs} "camouflage pattern".
 The helmet inside the bounding box clearly displays a military-style camouflage pattern with splotches of different colors.

Figure S10: **Representative dataset errors for positive captions.** Examples where the caption intends to describe a true absence of an attribute, but small objects, oclusions, or cluttered scenes make the decision borderline. These cases illustrate that the residual annotation noise in COVAND is dominated by inherently ambiguous instances.

Among the 78 disagreements, 23 are judged as true dataset errors and 55 as model errors. This yields an estimated annotation error rate of 2.3% on the audited sample, corresponding to 97.7% factual accuracy for COVAND. Most errors occur in visually ambiguous situations, such as fine-grained appearance attributes or partially occluded objects, rather than systematic failures of the generation pipeline.

Qualitative patterns. Fig. S9 and Fig. S10 illustrate typical error cases discovered by this audit. For negative captions, errors often arise when the "absent" attribute is present only in a subtle or non-prototypical form (e.g., skin-toned medical gloves that are hard to distinguish from bare hands), or when the bounding box tightly crops out context that would disambiguate the attribute. For positive captions, errors typically involve borderline cases where small accessories, distant objects, or strong reflections make it difficult to determine whether the attribute is truly absent in the marked region.

Overall, this analysis indicates that the remaining noise in COVAND is both quantitatively small and qualitatively concentrated in genuinely ambiguous instances, rather than reflecting a systematic self-consistency bias of the underlying generation procedure.

1242
1243
1244
1245
1246
1247
1248
1249
1250
1251
1252
1253
1254
1255
1256
1257
1258
1259
1260
1261
1262
1263
1264
1265
1266
1267
1268
1269
1270
1271
1272
1273
1274
1275
1276
1277
1278
1279
1280
1281
1282
1283
1284
1285
1286
1287
1288
1289
1290
1291
1292
1293
1294
1295

You are provided with an image in which the target object “<TARGET_PHRASE>” is highlighted using a red contoured bounding box. You are a vision-language model with advanced chain-of-thought reasoning. You must produce both negative and positive captions referencing the same main subject, “<TARGET_PHRASE>”.

Step 1) Summarize the highlighted bbox existing/missing contents (color, action, location, relationship, shape, texture, etc.):

[Existing Contents] Provide at least 3 short attribute or keyword items that describe SHOWN within the red bounding box.

- All contents should be CLEARLY CHECKED in image.
- Example: If the region corresponds to 'woman', you could include items like ['running at left lane', 'brown hair', 'blue shirt', 'jumping', 'holding a bat'].

[Absent Contents] Provide at least 3 short attribute or keyword items that describe NOT in the red bounding box.

- All contents should be CLEARLY MISSING in image, but somewhat relevant to the situation.
- Example: If the region corresponds to 'A woman in a blue shirt rides a bicycle', you could include items like ['helmet', 'glasses', 'red hoodie'], if all items are not in the image.

Step 2) For selected content items from step 1, produce exactly ONE negative caption and ONE positive caption with negation expressions (e.g. 'no', 'not', 'never', 'without', 'un-', ...). Each caption should be about the bounding box's main subject (“<TARGET_PHRASE>” in the red bbox) as the focus.

[Negative caption]: Caption that mismatched with the target region by combining negation expression and existing content item.

- (1) Must contain a negation expression with Existing Contents.
- (2) Keep it a single sentence or phrase, but it can be descriptive on target region.
- (3) Example: If existing contents are ['man', 'blue shirt', 'hat'] -> select 'hat'
=> 'A man without hat on his head.' ('hat' with 'without')
If existing contents are ['plate', 'on the top', 'black', 'near the woman']
=> select 'near the woman' => 'A black plate is not located near the woman.'

[Positive caption]: Caption that match with target region containing absent concepts with negation expressions.

- (1) Must contain a negation expression with Absent Contents.
- (2) Keep it a single sentence or phrase, which is actually present or relevant.
- (3) Example: If absent contents are ['helmet', 'glasses', 'red hoodie'] => select 'red hoodie',
you could say 'A woman without a red hoodie rides a bicycle.'

Step 3) Provide verification for each caption:

- After each negative or positive caption, include a short 'verification' string that clarifies why it is truly negative or positive, focusing on the use of the negation.
- Negative check: (1) Does it contain a negation expression? (2) Does it contain the existing item from Step 1? (3) Does it mismatch with the bounding box contents?
- Positive check: (1) Does it contain a negation expression? (2) Does it contain the absent item from Step 1? (3) Is that negation absent from the bounding box, but thematically relevant?

IMPORTANT:

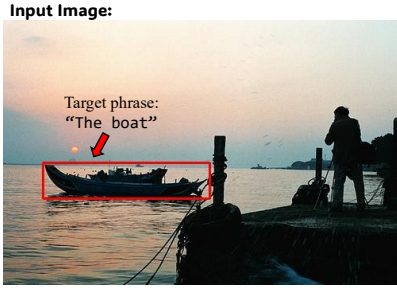
- Keep each caption to one sentence. Natural, fluent English with a bit of descriptive detail is encouraged.
- Your bbox_contents and subsequent captions should provide unique or distinguishing details specifically about the object in the target region, ensuring that they do not unintentionally refer to objects or attributes that lie outside of this indicated region.
- Return your final answer in a JSON structure with the following schema:

```
{
  "steps": [ { "explanation": "...", "output": "...", ... }, ... ],
  "bbox_contents": { "existing": [ ... ], "absent": [ ... ] },
  "pairs": [
    {
      "content_item": {
        "existing": "<one existing item>",
        "absent": "<one absent item>"
      },
      "negative_caption": "...",
      "negative_verification": "...",
      "positive_caption": "...",
      "positive_verification": "...
    }
  ]
}
```

You should reveal your chain-of-thought in steps[1,2,3], but keep it concise and do not mention about visual prompt in the final output sentences. Please identify at least 3 existing/missing items (other than the main subject) in that region, then select one for generating negative/positive caption pairs with verification. Use the JSON schema described above.

Figure S11: **Prompt for Three-step CoT Negation Caption Generation.** Our prompt guides the model to systematically (1) extract present and absent attributes from visually highlighted regions, (2) generate complementary negative and positive captions with explicit negation markers, and (3) verify semantic alignment through logical validation.

1296
1297
1298
1299
1300
1301
1302
1303
1304
1305
1306
1307
1308
1309
1310
1311
1312
1313
1314
1315
1316
1317
1318
1319
1320
1321
1322
1323
1324
1325
1326
1327
1328
1329
1330
1331
1332
1333
1334
1335
1336
1337
1338
1339
1340
1341
1342
1343
1344
1345
1346
1347
1348
1349



STEP 1 Summarize the highlighted bbox existing/missing contents

A_{pres} : ["dark silhouette", "still water reflection", "multiple antennas"]
 A_{abs} : ["bright decorations", "passenger activity", "painted details"]

STEP 2 For selected content items from step 1, produce negative and positive caption with negation expressions

C_{neg} : "The boat does **not** appear as a dark silhouette against the sunrise."
 C_{pos} : "The boat is shown **without** any bright decorations along its structure."

STEP 3 Provide verification for each caption

V_{neg} : "This caption uses 'not' with 'dark silhouette,' misrepresenting the boat's visual attribute."
 V_{pos} : "This caption uses 'without' with 'bright decorations,' confirming its absence in the bounding box."



STEP 1 Summarize the highlighted bbox existing/missing contents

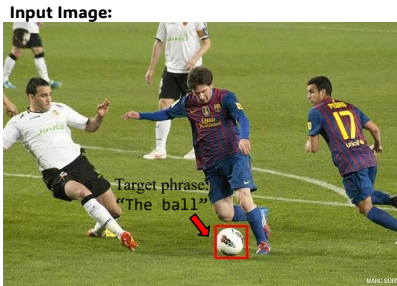
A_{pres} : ["white beard", "**blue cap**", "standing"]
 A_{abs} : ["gloves", "**glasses**", "apron"]

STEP 2 For selected content items from step 1, produce negative and positive caption with negation expressions

C_{neg} : "A man **without** a blue cap on his head."
 C_{pos} : "A man **without** glasses is standing in the doorway."

STEP 3 Provide verification for each caption

V_{neg} : "It contains a negation ('without') and the existing item ('blue cap'), which mismatches because the man clearly wears a blue cap."
 V_{pos} : "It contains a negation ('without') and the absent item ('glasses'), which is absent from the image and relevant to the setting."



STEP 1 Summarize the highlighted bbox existing/missing contents

A_{pres} : ["round", "black and white", "**logo**"]
 A_{abs} : ["net", "grass", "**foot touching**"]

STEP 2 For selected content items from step 1, produce negative and positive caption with negation expressions

C_{neg} : "The ball has **no** visible logo on it."
 C_{pos} : "The ball shows **no** foot touching by any player on the field."

STEP 3 Provide verification for each caption

V_{neg} : "Negative Verification: (1) Yes, it contains a negation. (2) Yes, it contains 'logo'. (3) Yes, it mismatches because the ball does have a logo."
 V_{pos} : "Positive Verification: (1) Yes, it contains a negation. (2) Yes, it contains 'foot touching'. (3) Yes, it is absent but relevant to a ball."



STEP 1 Summarize the highlighted bbox existing/missing contents

A_{pres} : ["**beige hat**", "pattern", "wide brim"]
 A_{abs} : ["**letters**", "passenger activity", "painted details"]

STEP 2 For selected content items from step 1, produce negative and positive caption with negation expressions

C_{neg} : "The woman is **not** wearing a beige hat atop her head."
 C_{pos} : "The hat on her head is **without** a letters."

STEP 3 Provide verification for each caption

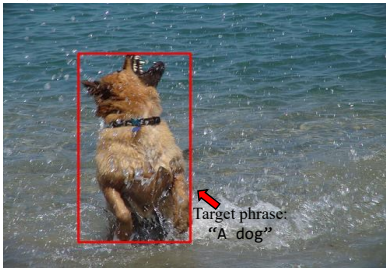
V_{neg} : "(1) Contains 'not' for negation. (2) Refers to 'beige hat'. (3) Contradicts the visual content, making it negative."
 V_{pos} : "(1) Contains 'without' for negation. (2) Refers to 'letters' as absent. (3) The absence of a logo is true and contextually relevant."

Figure S12: Examples of COVAND with 3-step CoT Caption Generation (1). Example images and corresponding captions. Text with blue is present attribute(A_{pres}) and pink is absent attribute(A_{abs}). In detail, <negation word>+< A_{pres} > can generate negative caption(C_{neg}) and <negation word>+< A_{abs} > can generate positive caption(C_{pos}).

1350

1351

Input Image:



1352

1353

1354

1355

1356

1357

1358

1359

1360

1361

1362

1363

1364

1365

1366

1367

1368

1369

1370

1371

1372

1373

1374

Input Image:



Target phrase:
"Infant Boy"

1364

1365

1366

1367

1368

1369

1370

1371

1372

1373

1374

STEP 1

Summarize the highlighted bbox existing/missing contents



A_{pres} : ["wet fur", "wearing a collar", "looking upward"]
 A_{abs} : ["clothing accessories", "a leash", "an obstacle"]

STEP 2

For selected content items from step 1, produce negative and positive caption with negation expressions



C_{neg} : "A dog that is **not** looking upward."
 C_{pos} : "A dog **without** a leash is standing in the water."

STEP 3

Provide verification for each caption



V_{neg} : "This caption is negative as it uses a negation expression with an existing attribute, mismatching the observed orientation of the dog."
 V_{pos} : "This caption is positive as it uses a negation expression for an absent attribute where no leash is visible, matching the lack of such an item."

Figure S13: Examples of COVAND with 3-step CoT Caption Generation (2). Example images and corresponding captions. Text with blue is present attribute(A_{pres}) and pink is absent attribute(A_{abs}). In detail, <negation word>+< A_{pres} > can generate negative caption(C_{neg}) and <negation word>+< A_{abs} > can generate positive caption(C_{pos}).

1375

1376

1377

1378

1379

1380

1381

1382

1383

1384

1385

1386

1387

1388

1389

1390

1391

1392

1393

1394

1395

1396

1397

1398

1399

1400

1401

1402

1403



Figure S14: Examples of Visual Prompt on VQA Alignments. We apply alphabetical region labeling to all bounding boxes that share the target phrase type by assigning distinct markers (A, B, C, . . .) to each instance with red bounding boxes.

1404
1405
1406
1407
1408
1409
1410
1411
1412
1413
1414
1415
1416
1417
1418
1419
1420
1421
1422
1423
1424
1425
1426
1427
1428
1429
1430
1431
1432
1433
1434
1435
1436
1437
1438
1439
1440
1441
1442
1443
1444
1445
1446
1447
1448
1449
1450
1451
1452
1453
1454
1455
1456
1457

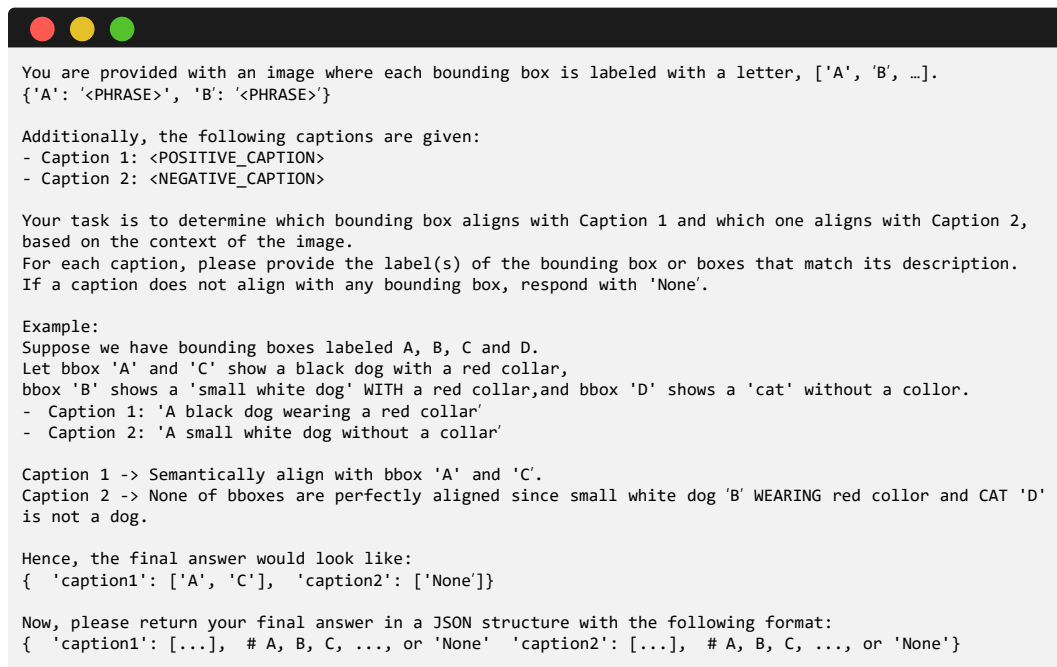


Figure S15: **Prompt for VQA Alignment.** Our alignment process with (1) labeling all candidate bounding boxes with alphabetical markers, and (2) querying the VQA model to determine precise correspondences between generated captions and visually annotated regions.

1458
1459
1460
1461
1462
1463
1464
1465
1466
1467
1468
1469
1470
1471
1472
1473
1474
1475
1476
1477
1478
1479
1480
1481
1482
1483
1484
1485
1486
1487
1488
1489
1490
1491
1492
1493
1494
1495
1496
1497
1498
1499
1500
1501
1502
1503
1504
1505
1506
1507
1508
1509
1510
1511

Example 1: Formal Costume
 Target phrase: "formal costume"
 3-step CoT Negation Caption Generation:
 C_{neg} : "The formal costume lacks a red dupatta."
 C_{pos} : "The formal costume without a hat."
 VQA-based Caption Alignment:
 Q: Which bbox aligns with given captions?
 C_{neg} : None
 C_{pos} : A

Example 2: Light Brown Dog
 Target phrase: "light brown dog"
 3-step CoT Negation Caption Generation:
 C_{neg} : "A light brown dog is not wearing a red collar while playing."
 C_{pos} : "A light brown dog is playing without a ball in sight."
 VQA-based Caption Alignment:
 Q: Which bbox aligns with given captions?
 C_{neg} : None
 C_{pos} : A

Example 3: Dog Jumping
 Target phrase: "dog"
 3-step CoT Negation Caption Generation:
 C_{neg} : "The dog is not in a jumping pose."
 C_{pos} : "The dog is playing without a leash."
 VQA-based Caption Alignment:
 Q: Which bbox aligns with given captions?
 C_{neg} : A
 C_{pos} : A

Example 4: Kids Running
 Target phrase: "kids"
 3-step CoT Negation Caption Generation:
 C_{neg} : "A kid not wearing a green shirt runs along the sidewalk."
 C_{pos} : "A kid runs without a jacket along the sidewalk."
 VQA-based Caption Alignment:
 Q: Which bbox aligns with given captions?
 C_{neg} : A, B
 C_{pos} : A, B

Example 5: Young Boys Playing Guitars
 Target phrase: "young boys"
 3-step CoT Negation Caption Generation:
 C_{neg} : "The young boys are not playing any guitars."
 C_{pos} : "The young boys perform without any visible music sheets."
 VQA-based Caption Alignment:
 Q: Which bbox aligns with given captions?
 C_{neg} : None
 C_{pos} : A, B, C

Figure S16: **Examples of CoVAND.** Example images for the 3-step CoT Negation Caption Generation and the VQA alignment are needed. The VQA alignment step is only executed when there are multiple instances with the same phrase type.

1512
 1513
 1514
 1515
 1516
 1517
 1518
 1519
 1520
 1521
 1522
 1523
 1524
 1525
 1526
 1527
 1528
 1529
 1530
 1531
 1532
 1533
 1534
 1535
 1536
 1537
 1538
 1539
 1540
 1541
 1542
 1543
 1544
 1545
 1546
 1547
 1548
 1549
 1550
 1551
 1552
 1553
 1554
 1555
 1556
 1557
 1558
 1559
 1560
 1561
 1562
 1563
 1564
 1565

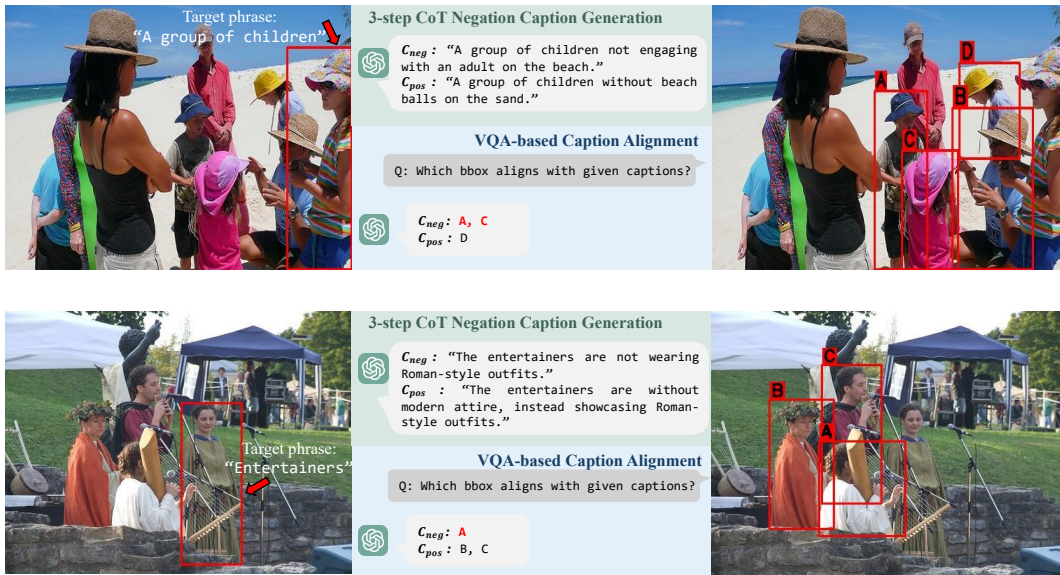


Figure S17: **Error on COVAND.** VQA alignment occasionally fails when instances are densely clustered, making it difficult to determine which instance each visual prompt references.

B IMPLEMENTATION DETAILS

B.1 GROUNDING DINO MODEL

Our implementation is built upon the Grounding DINO architecture (Liu et al., 2024b; Zuwei Long, 2023), which employs a dual-encoder-single-decoder design for vision-language understanding. For efficient fine-tuning towards negation understanding, we apply LoRA (Hu et al., 2022) to specific layers of the cross-modality decoder. The Grounding DINO consists of several key components:

- An image backbone (Swin Transformer (Liu et al., 2021)) for visual feature extraction
- A text backbone (BERT (Devlin et al., 2019)) for textual feature encoding
- A feature enhancer with self-attention and cross-attention mechanisms
- A language-guided query selection module that initializes query embeddings
- A cross-modality decoder that refines object detection based on both visual and text

We implement parameter-efficient fine-tuning by applying LoRA to deep layers (the final three cross-attention layers in the cross-modality decoder). This strategic placement allows us to modify how the model integrates negation cues from text with visual features while preserving pre-trained knowledge in earlier layers. Specifically, we insert LoRA only into the query (Q) and value (V) projections of the **text cross-attention**; the image deformable cross-attention and the self-attention blocks remain unchanged. The addition of ReLU activation between the down-projection and up-projection matrices, similar to (Chen et al., 2022), enhances the model’s ability to capture non-linear relationships between negation cues and visual features. In Grounding DINO’s cross-attention, the interactions operate as follows:

- **Image Cross-Attention:**
 - Query (Q): the updated cross-modality query from the preceding self-attention layer
 - Key (K) and Value (V): the image features processed through the feature enhancer
- **Text Cross-Attention:**
 - Query (Q): the output from the image cross-attention layer
 - Key (K) and Value (V): text features encoding language information

Figure S18 reveals critical insights into the optimal placement of LoRA modules (Boenisch et al., 2025) for negation understanding. The baseline model (Figure S18a) shows a strong bias toward Special tokens across all decoder blocks, with negation cues receiving minimal attention. When we apply LoRA to shallow blocks (Figure S18b), negation tokens initially receive higher attention weights in blocks 0-2, but this effect rapidly diminishes in the later blocks where attention to negation drops.

In contrast, when we apply LoRA to deep blocks (Figure S18c), the model maintains consistent attention to negation tokens through blocks. This pattern persists through the final detection heads, explaining the superior negation-aware detection performance. Some works (Gao et al., 2025; 2024; Seputis et al., 2024) further validate our approach by demonstrating that allocation of adaptation capacity to mid-to-late transformer layers yields optimal results for complex semantic tasks.

With the addition of NEGToME (Figure S18d), attention to negation tokens increases consistently across all blocks, with particular amplification in the final blocks where detection decisions are made. This confirms that our token merging strategy effectively preserves negation signals throughout the entire network, even in early blocks that did not receive LoRA adaptation. The combined effect creates a consistent processing path for negation cues from text encoding through to final detection, explaining the significant performance improvements observed in the OVDEval and D³ benchmarks.

Together, these adaptations enable our model to effectively capture the semantics of negation by enhancing the cross-modal integration of negation cues with their corresponding visual attributes, resulting in more accurate detection under negation scenarios.

Compared with the tiny model of Grounding DINO baseline, we need merely 0.005% trainable parameters to capture negation cues effectively, as in Table S7. To keep the tiny model within the

1620
1621
1622
1623
1624
1625
1626
1627
1628
1629
1630
1631
1632
1633
1634
1635
1636
1637
1638
1639
1640
1641
1642
1643
1644
1645
1646
1647
1648
1649
1650
1651
1652
1653
1654
1655
1656
1657
1658
1659
1660
1661
1662
1663
1664
1665
1666
1667
1668
1669
1670
1671
1672
1673

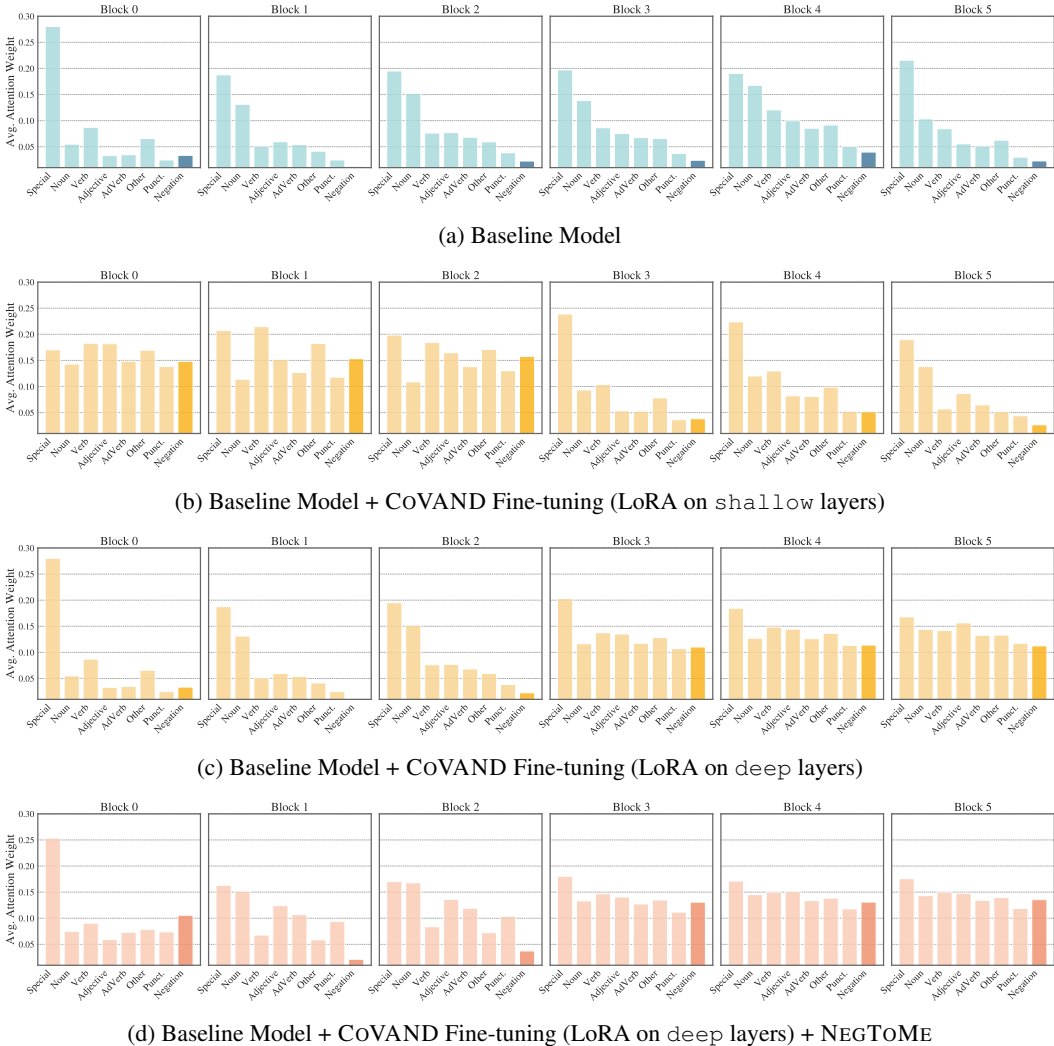


Figure S18: **Average Attention Weights by Decoder Blocks.** We only update the LoRA modules while freezing other layers for fine-tuning. Placement of LoRA, *shallow* means LoRA located on early decoder blocks (0-2) and *deep* means LoRA located on latter decoder blocks (3-5).

Table S6: **OVDEval-Negation Evaluation.** Performance on Grounding DINO tiny model.

	AP	NMS-AP (Yao et al., 2024)	FPR
G-DINO-T (Liu et al., 2024b)	48.5	22.8	54.0
+ Ours	51.1 (+2.6)	23.3 (+0.5)	42.5 (-11.5)

same 0.005% budget, we attach LoRA adapters to the 4 and 5 text cross-attention blocks of the decoder. Our lightweight adaptation yields a consistent performance gain: +2.6 AP and +0.5 NMS-AP, while slashing the False-Positive Rate (FPR) by **11.5%** as in Table S6. Although AP and NMS-AP improvements are moderate, they are achieved without sacrificing any metric; in fact, every reported score is on par with, or better than, the baseline, indicating that our negation-centric tuning does not degrade the detector’s general ability.

Table S7: **Trainable Parameter Ratio.** The table compares the total model size with the number of LoRA-tuned parameters for each detector and backbone pair. During fine-tuning on CoVAND, only the LoRA layers are trainable, with all other layers kept frozen with their pretrained weights.

	Image Backbone	Total Param.	LoRA Param.	Ratio (%)
G-DINO-T (Liu et al., 2024b)	Swin-T (28.8M)	173M	8.2k	0.005
G-DINO-B (Liu et al., 2024b)	Swin-B (88M)	233M	12.3k	0.005
APE-Ti (Shen et al., 2024)	ViT-Ti (5.8M)	771M	129k	0.017
APE-L (Shen et al., 2024)	ViT-L (307M)	1B	129k	0.012
Qwen-2.5-VL-3B (Bai et al., 2025)	ViT-H (632M)	3.8B	77k	0.002

B.2 APE MODEL

Our implementation builds upon the APE framework (Shen et al., 2024), a universal visual perception model that unifies detection, segmentation, and grounding through instance-level region-sentence alignment. The architecture features several key innovations:

- A vision backbone (ViT-L (Dosovitskiy et al., 2020)) pretrained with EVA-CLIP (Sun et al., 2023) for visual feature extraction
- A text encoder (EVA02-CLIP (Fang et al., 2024)) processing both categorical vocabularies and free-form descriptions
- A gated cross-modality interaction module that fuses visual and text features
- A transformer decoder with deformable attention (Zhu et al., 2020) for joint reasoning

APE introduces a novel gated fusion mechanism that efficiently handles thousands of prompts per forward pass. Unlike previous approaches that directly fuse all text features (Li et al., 2022), APE implements conditional interaction paths:

$$\hat{V} = \begin{cases} V + \text{Attn}(V, P_{\text{voc}}) & \text{for vocabulary prompts} \\ \text{Attn}(V, P_{\text{sen}}) & \text{for sentence descriptions} \end{cases} \quad (4)$$

where V denotes visual features and P represents text embeddings. This gating strategy reduces FLOPs compared to GLIP-style fusion (Li et al., 2022). The model processes inputs at 1,024 pixel resolution using AdamW optimization (Loshchilov & Hutter, 2017) with learning rate 0.0005 and weight decay 0.05. We employ large-scale jittering augmentation (Ghiasi et al., 2021) with random scales from 0.1 to 2.0. We train APE-Ti models with four A6000 GPUs with a batch size of 4.

We apply LoRA exclusively to the encoder’s cross-attention layers where visual and text features interact. This targeted adaptation modifies only 0.017% of APE’s parameters as in Table S7. Despite APE-L’s strong theoretical performance, its 1B parameters exceed the 48GB memory capacity of NVIDIA A6000 GPUs during training. We therefore focus on APE-Ti, which achieves 32.5 AP on D³ while maintaining practical deployability.

B.3 QWEN-2.5-VL MODEL

In addition to dedicated detectors, we test our method’s generalizability on a powerful Multimodal Large Language Model (MLLM), Qwen-2.5-VL (Bai et al., 2025). Unlike dual-encoder architectures, Qwen-2.5-VL is an end-to-end model that directly processes interleaved image and text data. As detailed in its technical report, the architecture consists of three main components:

- A Vision Transformer (ViT-H) that is redesigned and trained from scratch to handle native resolution inputs. For efficiency, it incorporates windowed attention in most layers, with full self-attention only in specific blocks. The ViT architecture is also updated with RMSNorm and SwiGLU activations to align with modern LLM design principles.
- An MLP-based Vision-Language Merger that compresses spatially adjacent patch features before feeding them into the language model, enhancing computational efficiency.

- A Large Language Model decoder based on the Qwen2.5 architecture, which performs unified reasoning over the combined multimodal input and generates responses, including object coordinates for detection tasks.

For parameter-efficient fine-tuning, we again employ LoRA, strategically targeting the `deep` layers of the LLM decoder to enhance its negation reasoning without disturbing its foundational knowledge. Based on our experimental setup, LoRA adapters are specifically injected into the query (`q_proj`) and value (`v_proj`) projections of the self-attention modules within layers (15, 24, 30). This targeted placement is designed to modulate how the model integrates visual information with textual negation cues in its higher-level semantic reasoning stages. We configure the LoRA adapters with a rank r of 4 and a dropout probability of 0.05.

Following the execution script, the Qwen-2.5-VL-3B model is fine-tuned for 1 epoch on our COVAND dataset on H200 GPU. We use a learning rate of $5e - 5$ with the AdamW optimizer (Loshchilov & Hutter, 2017) and a per-device batch size of 32, with 2 gradient accumulation steps, totaling an effective batch size of 64. The model is trained using bfloat16 mixed-precision. During this process, all original model parameters—including the ViT, MLP merger, and LLM backbone—are kept frozen; only the injected LoRA adapter weights are updated.

C EXTENDED RELATED WORK

C.1 DATASET CONSTRUCTION WITH CHAIN-OF-THOUGHT REASONING

Chain-of-Thought (CoT) based data generation has emerged as a critical methodology for constructing high-quality datasets, particularly for tasks requiring multi-step reasoning. Early work in this domain relied heavily on manual annotation or rule-based generation, but recent advances have automated and scaled CoT-based dataset construction through Large Language Models (LLMs).

Systematic CoT Pipeline Design The construction of CoT datasets requires careful consideration of quality and scale trade-offs. VideoEspresso (Han et al., 2025) demonstrates a systematic approach to automatic CoT dataset generation, employing a three-stage pipeline: (1) semantic-aware key information extraction using frame-level captioning (Kazakos et al., 2025), (2) multi-frame question-answer pair construction guided by carefully designed prompts, and (3) multimodal CoT annotation with spatial and temporal grounding (Kim et al., 2025).

This pipeline bridges the gap between manual annotation and fully automated generation by leveraging LLMs to produce reasoning chains (Lee et al., 2024; Tan et al., 2024) while maintaining consistency and factual accuracy through iterative quality filtering with an auxiliary LLM validator (Wang et al., 2025b; Chen et al., 2025d). The approach implements a redundancy removal mechanism using semantic similarity (Abbas et al., 2023) to filter out low-quality data, achieving 203,546 high-quality QA pairs with fine-grained CoT annotations. Furthermore, external validation tools (Findeis et al., 2025) are employed to ground generated annotations in visual evidence, ensuring both consistency across temporal boundaries and factual accuracy of intermediate reasoning steps.

Information-Theoretic Framework for CoT Evaluation Understanding the quality of intermediate reasoning steps in CoT chains is essential for constructing reliable datasets. Recent works (Ton et al., 2024) propose an information-theoretic framework that formalizes CoT reasoning through the lens of information theory (Xiao et al., 2025), enabling the identification of failure modes without annotated CoT data. This theoretical foundation is grounded in process supervision paradigms (Lightman et al., 2023; Jia et al., 2025).

Their key contribution is the concept of information-gain at each reasoning step: a correct step should provide meaningful information toward predicting the final answer. By training a supervisor model to estimate conditional mutual information between intermediate steps and the final answer, they can quantify the contribution of each step without expensive human annotation. This approach outperforms outcome-based reward models (Lightman et al., 2023) and Math-Shepherd on detecting erroneous reasoning steps (Chen et al., 2025b).

The framework extends toward mechanistic interpretability through sparse autoencoders and activation patching (Chen et al., 2025c). These techniques reveal that CoT induces interpretable compu-

tational structures in larger models, with domain-specific causal patterns (Zhao et al., 2025). This mechanistic analysis validates that intermediate steps reflect genuine internal computation (FU et al., 2025).

The framework extends beyond simple accuracy metrics to provide step-wise interpretability (Hanna et al., 2025) and identifies unidentifiable sub-tasks—those which the model has not learned from training data (Muhammed et al., 2025). By combining information-theoretic analysis with causal structure verification, the framework creates a comprehensive evaluation pipeline grounded in both statistical and mechanistic principles.

Synthesis for COVAND Dataset Construction Drawing from these insights, our COVAND dataset construction pipeline incorporates: (1) systematic 3-step CoT prompts guided by information-theoretic principles to ensure each step contributes meaningful information, (2) multi-level quality verification using both LLM-based filtering and human review to ensure faithfulness, (3) validation through external VQA models to confirm region-level alignment accuracy, and (4) careful consideration of model scale effects by selecting sufficiently large models for CoT generation. This comprehensive approach ensures that COVAND provides high-quality, instance-grounded negation data where the reasoning process genuinely reflects the model’s internal understanding.

C.2 VISUAL GROUNDING AND REGION-LEVEL ALIGNMENT IN VQA

Visual grounding, which is the task of localizing image regions corresponding to textual descriptions, plays a crucial role in connecting language-based reasoning to visual content. This capability is particularly important for our NEGTOE module, which grounds text tokens to image regions to implement negation-aware token merging.

Visual Grounding Methods and Evaluation Visual grounding has evolved from CNN-based two-stage pipelines to unified transformer-based end-to-end frameworks. TransVG (Deng et al., 2021) pioneered transformer-based visual grounding by performing intra- and inter-modality relation reasoning homogeneously. Recent advances further improved this by moving toward multi-task grounding architectures that jointly perform localization and segmentation (Dai et al., 2025) and leveraging coarse-to-fine consistency constraints. A comprehensive survey on visual grounding (Xiao et al., 2024) systematizes this evolution and identifies critical research directions, including grounding multimodal LLMs and generalized visual grounding.

A key insight is that visual grounding can be performed efficiently without fine-tuning. Contrastive Region Guidance (CRG) (Wan et al., 2024) introduces a training-free guidance method that enables open-source VLMs to respond to visual prompts by contrasting model outputs with and without region masking. CRG achieves up to 11.1% absolute accuracy improvements across diverse region-based tasks, demonstrating that pre-trained VLM representations already encode spatial information. This aligns with our design choice of using lightweight region guidance rather than expensive fine-tuning, and CRG complements our token-merging approach by providing model-driven region importance weighting.

VQA-Based Visual Grounding Visual Question Answering (VQA) provides a natural framework for generating region-level annotations. Some works (Shrestha et al., 2020a;b) show that visual grounding mechanisms are essential for explaining VQA predictions, bridging the gap between model confidence and spatial localization. More recent work (Reich & Schultz, 2024) uncovers the full potential of visual grounding methods in VQA, revealing that region-level understanding significantly improves multi-hop reasoning capabilities. Learning visual grounding from generative VLMs (Wang et al., 2025a) demonstrates that modern generative models can implicitly learn spatial correspondences, which our approach leverages by using model-generated region descriptions.

Spatial vs. Semantic Matching A fundamental distinction in visual grounding exists between spatial matching (geometric alignment) and semantic matching (concept alignment). Recent works (Chen et al., 2023; Daxberger et al., 2025) demonstrate that semantic alignment based on visual-linguistic correspondence often outperforms purely spatial approaches. Our VQA-based validation mechanism employs semantic matching by querying the model about object presence and

1836 roles in specific regions, effectively combining spatial information (bounding boxes) with semantic
1837 understanding (question-answer consistency).
1838

1839 **Grounding for Instance-Level Negation** For instance-grounded negation understanding, precise
1840 visual grounding is critical. The COVAND dataset construction process uses region-level VQA
1841 to ensure that when we assert “not X,” the region boundaries are accurately localized and the ab-
1842 sence claim is semantically verified. This region-centric approach differs from image-level negation
1843 understanding, which cannot distinguish between objects appearing in different spatial contexts.
1844

1845 C.3 PARAMETER-EFFICIENT FINE-TUNING FOR VISION-LANGUAGE MODELS

1846 Large vision-language models contain billions of parameters, making full fine-tuning computation-
1847 ally prohibitive. Parameter-efficient fine-tuning (PEFT) techniques enable adaptation with minimal
1848 additional parameters, a critical requirement for our NEGTOPE adapter design.
1849

1850 **Low-Rank Adaptation (LoRA) and Variants** LoRA (Hu et al., 2022) introduced a breakthrough
1851 approach decomposing weight updates into low-rank matrices $W = W_0 + AB^T$, where $A \in \mathbb{R}^{d \times r}$
1852 and $B \in \mathbb{R}^{r \times d}$ with rank $r \ll d$. This reduces trainable parameters from $O(d^2)$ to $O(dr)$. For CLIP-
1853 like models, LoRA has proven highly effective in few-shot scenarios. Low-rank few-shot adaptation
1854 of vision-language models (Zanella & Ben Ayed, 2024) empirically demonstrates that CLIP-LoRA
1855 achieves substantial improvements over prompt-learning and adapter-based approaches across 11
1856 datasets while maintaining consistent hyperparameters across all tasks, effectively democratizing
1857 few-shot VLM adaptation without task-specific tuning.

1858 A comprehensive PEFT survey (Han et al., 2024) provides systematic evaluation of PEFT algorithms
1859 and their computational overhead, revealing that LoRA remains competitive against more complex
1860 PEFT variants (prefix tuning, adapters, prompt tuning) for vision-language adaptation, particularly
1861 when strategically applied to specific layer types. However, the low-rank constraint limits expres-
1862 sivity on complex tasks. DoRA (Liu et al., 2024a), a weight-decomposed variant, decouples weight
1863 matrices into independent magnitude and direction components, emulating full fine-tuning dynam-
1864 ics more faithfully. DoRA consistently outperforms LoRA on vision-language tasks including visual
1865 instruction tuning (Liu et al., 2024a).

1866 **Strategic Layer-Wise Adaptation** Not all layers benefit equally from fine-tuning. Analysis of
1867 vision-language architectures reveals that cross-modal attention layers are critical for semantic align-
1868 ment. Full-rank parameter-efficient fine-tuning (Albert et al., 2025) proposes RandLoRA, which
1869 performs full-rank updates via learned linear combinations of low-rank random matrices. Rand-
1870 LoRA significantly reduces the performance gap between LoRA and standard fine-tuning, particu-
1871 larly on vision-language tasks, demonstrating that when higher ranks are required, full-rank updates
1872 substantially outperform low-rank approximations.

1873 Layer-wise learning strategies further refine adaptation. Layer-wise auto-weighting (Park et al.,
1874 2024a) employs Fisher Information Matrix (FIM) to autonomously identify which layers require
1875 preservation or concentrated adaptation, enabling more efficient non-stationary test-time adapta-
1876 tion. For our approach, we strategically apply LoRA to deep cross-attention layers where negation-
1877 specific reasoning is encoded, achieving a balance between expressiveness and efficiency. Addi-
1878 tionally, data-efficient instruction tuning (Naharas et al., 2025) proves that examples with similar
1879 cross-modal attention matrices have similar gradients, informing our layer selection strategy: layers
1880 exhibiting high cross-modal attention variance are most critical for negation grounding.
1881

1882 **Fine-Grained Semantic Alignment** Task-specific semantic alignment requires minimal paramet-
1883 ers but careful design. A parameter-efficient prompt learning method (Guo et al., 2025) achieves
1884 fine-grained semantic alignment using only a few additional parameters. Their key insight is that
1885 semantic-level objectives require less parameter capacity than low-level pixel matching, particularly
1886 when combined with well-designed prompt templates and explicit semantic constraints.

1887 For semantic gating in transformers, Value-State Gated Attention (Bu et al., 2025) introduces learn-
1888 able, data-dependent gates computed from value vectors to modulate token contributions based on
1889 semantic importance. This mechanism directly informs NEGTOPE’s token importance weighting:
by learning task-specific gates that suppress irrelevant tokens and amplify negation-bearing tokens,

we achieve semantic specialization with minimal overhead. Dynamic Mask Attention (Zhang et al., 2025) extends this by using soft-gating masks and content-aware mask generation based on value representations, enabling fine-grained token importance capture without binary keep-or-drop decisions.

Negation-Specific Adapter Design While most PEFT work addresses general-purpose adaptation, negation understanding requires specialized reasoning. Our NEGTOPE module combines LoRA’s parameter efficiency with negation-aware token merging, creating a compact yet semantically rich adaptation.

The negation-boost mechanism in token merging acts as a learned semantic gating function, allocating more computational resources to tokens representing negated concepts. This semantic specialization follows principles from hierarchical inductive transfer for continual learning (Feng et al., 2022), which demonstrates that separating base adapters (capturing general knowledge) from task-specific adapters (capturing task-specialized reasoning) prevents interference and improves performance on specialized tasks. By analogy, NEGTOPE’s selective token enhancement prevents general cross-modal attention from suppressing negation signals.

Synthesis: Efficient Negation-Aware Adaptation Our PEFT strategy for NEGTOPE combines: (1) *LoRA efficiency*: strategic application to cross-modal attention layers, (2) *full-rank expressivity*: capturing complex negation-direction mappings, (3) *semantic gating*: value-state aware token importance weighting, and (4) *hierarchical structure*: base cross-modal adaptation and task-specific negation enhancement. This integrated approach ensures parameter efficiency while providing sufficient expressivity for negation-aware semantic reasoning, critical for learning instance-grounded negation in vision-language tasks.

C.4 COMPOSITIONAL REASONING IN VISION-LANGUAGE TASKS

Compositional reasoning—understanding how simple concepts combine to form complex meanings—is fundamental to negation understanding. Negation is inherently compositional: “not red” requires first identifying “red” then applying the negation operator.

Compositional Generalization in Vision-Language Models A critical gap exists between training and test distributions: models trained on one compositional split often fail on others, revealing weak compositional generalization. An empirical study on compositional generalization in VLMs (Li et al., 2024a) shows that current models rely primarily on linguistic priors rather than visual information, causing benchmarks to favor pure language models. To overcome this limitation, researchers propose evaluation frameworks without linguistic priors, forcing models to ground compositional reasoning in actual visual content.

Systematic compositional probing studies (Li et al., 2025c) evaluate whether RL-trained VLMs inherit compositional capabilities from LLMs. Key findings reveal: (1) RL-trained models outperform SFT-only models on compositional generalization, (2) VLMs struggle to generalize compositionally under cross-modal and cross-task scenarios despite strong individual-task performance, and (3) enforcing models to explicitly ground visual content before reasoning (e.g., caption-before-thinking with visual grounding) yields notable gains. These findings directly motivate our explicit chain-of-thought (CoT) dataset construction: by forcing models to describe what negation means in specific regions before making predictions, we encourage true compositional understanding rather than shortcut learning.

Out-of-distribution generalization in LLMs is fundamentally tied to compositional structures internally achieved through aligned principal subspaces in self-attention layers (Song et al., 2025). This analysis suggests that models composing two self-attention layers can learn rules and generalize to novel tasks—a principle we leverage by designing NEGTOPE to operate at intermediate layers where compositional negation reasoning naturally emerges.

From Objects to Events: Temporal Compositional Reasoning Event-level reasoning extends compositional understanding beyond static attributes to temporal dynamics. Compositional event reasoning requires understanding object interactions and temporal sequences. Recent work on

1944 diffusion-driven video scene graph generation (Chen et al., 2025a) demonstrates that detecting com-
 1945 plex temporal relations requires compositional reasoning about object trajectories and inter-frame
 1946 dependencies, achieved through iterative refinement of spatial-temporal embeddings. Video refer-
 1947 ring object segmentation (Xu et al., 2025) decomposes referring expressions into structured event
 1948 graphs with objects, relations, and temporal constraints, revealing that video-level negation requires
 1949 reasoning about event-level compositional patterns.

1950 Our 3-step CoT generation aligns with this event decomposition: each step performs a primitive
 1951 operation (object detection → region analysis → negation verification), mirroring the hierarchical
 1952 event reasoning paradigm. By explicitly grounding each reasoning step in concrete regions, CO-
 1953 VAND teaches models to compose negation patterns systematically rather than relying on spurious
 1954 correlations.

1955
 1956 **Attribute Binding and Multi-Object Reasoning** A central compositional challenge is correctly
 1957 binding attributes to objects (the binding problem). Scene graph generation literature (Chang et al.,
 1958 2021; Yang et al., 2024), identifies systematic failures in relational understanding. Video scene graph
 1959 generation with unbiased training (Li et al., 2025d) addresses these failures through visual-semantic
 1960 dual supervision, explicitly enforcing consistency between visual features and semantic relations.
 1961 For negation, this principle translates to enforcing consistency between negated object descriptions
 1962 and their spatial absence in images.

1963 **Multimodal Compositional Generalization** Retrieving semantically equivalent primitives across
 1964 modalities enhances compositional generalization. Multi-sourced compositional generalization in
 1965 VQA (Li et al., 2025b) proposes retrieval-augmented training where equivalent primitives from dif-
 1966 ferent modalities are aggregated to refine representations, improving generalization to novel compo-
 1967 sitions. For negation, this principle suggests that enforcing consistency between linguistic negation
 1968 descriptions and visual absence patterns (via VQA-based validation) teaches models to reason about
 1969 negation as a unified cross-modal compositional operator.

1970
 1971 **Systematic Generalization in Visual Reasoning** A benchmark for systematic generalization in
 1972 visual world models (Kim et al., 2023b) evaluates whether models perform visual imagination and
 1973 measure compositional generalization systematically. The benchmark reveals that even state-of-the-
 1974 art models fail on out-of-distribution compositional scenarios. Our approach mirrors this systematic
 1975 evaluation: by constructing COVAND with systematic variations across objects, attributes, and
 1976 negation types, we provide training data that encourages systematic rather than accidental general-
 1977 ization.

1978 **Synthesis: Compositional Negation as Structured Visual Reasoning** Our approach positions
 1979 negation as a compositional operator within a broader framework of structured visual reasoning.
 1980 By combining: (1) *explicit event decomposition* through 3-step CoT reasoning, (2) *visual-semantic*
 1981 *binding enforcement* via VQA validation, (3) *spurious correlation mitigation* through systematic
 1982 data variation, and (4) *out-of-distribution generalization* via consistent cross-modal mappings, CO-
 1983 VAND enables models to learn compositional negation patterns grounded in both visual evidence
 1984 and semantic structure. This compositional foundation, combined with NEGTOPE’s semantic-
 1985 aware token merging that respects the hierarchical structure of compositional reasoning, creates a
 1986 framework where negation understanding emerges from systematic compositional principles rather
 1987 than shallow surface-level negation cues.

1988 C.5 BIAS MITIGATION IN VISION-LANGUAGE MODELS

1989
 1990 Affirmative bias—the tendency to misinterpret negations as affirmations—represents a systematic
 1991 bias in VLM training data and architecture. Understanding and mitigating this bias is central to our
 1992 work.

1993
 1994 **Understanding Affirmative Bias in VLMs** The fundamental source of affirmative bias lies in
 1995 training data distribution. Most visual-linguistic corpora contain predominantly positive image-text
 1996 pairs: “dog in park,” “person running,” etc. Negative examples are rare, creating class imbalance
 1997 that models exploit through shortcut learning. DeAR (Seth et al., 2023) demonstrates that VLM bias
 can be partially mitigated by learning additive residual corrections to visual representations without

1998 retraining. However, their approach targets shallow social biases; negation bias requires deeper
1999 structural understanding.

2000 Recent work reveals that VLMs exhibit social biases including gender and racial stereotypes in
2001 their generative responses (Lan et al., 2025). More critically, fair-response reliability differs from
2002 accuracy: models may achieve high accuracy while exhibiting significantly lower fairness scores.
2003 This decoupling between performance and fairness motivates our multi-level debiasing strategy,
2004 where data-level, method-level, and evaluation-level components collectively address negation bias.
2005

2006 **Architectural Sources of Affirmative Bias** Bias is not merely a data problem but deeply embed-
2007 ded in architectural choices. Bias analysis in transformer attention heads (Yang et al., 2025) reveals
2008 that specific attention heads are responsible for encoding stereotypical biases; by identifying and
2009 masking high-bias heads, models achieve significant bias reduction without affecting language un-
2010 derstanding. This attention-head level analysis directly informs NEGTOPE’s design: our selective
2011 token merging operates at the semantic level, effectively masking attention patterns that suppress
2012 negation signals.

2013 **Shortcut Learning and Spurious Correlation** Models exploit spurious correlations—features
2014 coincidentally correlated with labels in training data—to achieve high training accuracy while gen-
2015 eralizing poorly to test data. Shortcut learning in LLMs (Du et al., 2023) identifies that models learn
2016 to associate demographic attributes with spurious features rather than learning genuine causal rela-
2017 tionships. For negation, this manifests as: models may learn that “absence of red” correlates with
2018 “dark backgrounds” rather than learning true negation semantics.

2019 **ShortcutProbe** (Zheng et al., 2025) introduces a post-hoc framework for identifying and mitigating
2020 spurious biases via prediction shortcuts in the model’s latent space, without requiring group labels.
2021 The key insight is that spurious correlations create non-generalizable prediction shortcuts that fail
2022 under distribution shift. Our CoVAND addresses this by systematically varying objects, attributes,
2023 and spatial configurations, forcing models to learn generalizable negation patterns rather than spuri-
2024 ous shortcuts. Furthermore, generative classifiers naturally avoid shortcut learning (Li et al., 2025a)
2025 by modeling all features rather than mainly spurious ones, suggesting an alternative avenue for ro-
2026 bust negation understanding.
2027

2028 **Synthetic Data Augmentation and Its Pitfalls** While data augmentation seems a natural solution,
2029 naive approaches can inherit and amplify existing biases. Decoupling augmentation bias in prompt
2030 learning for VLMs (Gerych et al., 2024) demonstrates that random negation (e.g., “not red” gener-
2031 ated from “red”) can create inconsistent training signals due to augmentation distribution mismatch.
2032 CoVAND addresses this by employing LLMs to generate semantically coherent negation examples
2033 with multi-step chain-of-thought reasoning verification, ensuring both linguistic consistency and
2034 visual grounding.

2035 **Handling imbalanced pseudolabels in VLMs** (Pang et al., 2025) reveals that models exhibit class-
2036 preference biases when generating pseudolabels for unlabeled data. Their proposed solution com-
2037 bines concept alignment with confusion-aware calibrated margins. Our CoVAND-derived dataset
2038 similarly enforces consistency through VQA validation and avoids concept confusion via systematic
2039 negation type variation.
2040

2041 **Bias Inheritance in LLM-Based Data Augmentation** LLM-based augmentation introduces new
2042 challenges: models inherit biases from their training distribution even when generating synthetic
2043 data (Li et al., 2025a). When an LLM generates “not sitting,” it may unconsciously preserve biases
2044 about typical sitting scenarios and demographic associations. Our solution combines LLM genera-
2045 tion with human review and VQA validation, creating a hybrid pipeline resistant to bias inheritance.
2046 This multi-stage validation mirrors fairness-aware domain adaptation for VLMs (Pang et al., 2025),
2047 which uses attribute-aware strategies to dynamically adapt to diverse demographics for equitable
2048 outcomes.
2049

2050 **Negation-Aware Test-Time Adaptation** Beyond training-time mitigation, test-time debiasing of-
2051 fers complementary benefits. BEND-VLM (Gerych et al., 2024) proposes nonlinear, fine-tuning-
free debiasing that tailors debiasing to each unique input without prior knowledge of the test set.

2052 While their approach targets social biases, the principle of input-specific bias correction directly ap-
 2053 plies to negation: negation scopes and interpretations vary contextually, so adaptive, query-specific
 2054 debiasing enhances robustness.

2055 Debiasing VLMs using backdoor learning (Pang et al., 2025) proposes learning backdoor patterns
 2056 that trigger debiased representations, enabling inference-time debiasing without model modifica-
 2057 tion. This technique complements our approach: while NEG-TOME merges tokens based on learned
 2058 negation patterns, backdoor triggers could provide additional control signals for negation-aware in-
 2059 ference.

2060
 2061 **Synthesis: Multi-Level Affirmative Bias Mitigation** Our comprehensive approach targets affir-
 2062 mative bias across multiple levels:

- 2063
 2064 1. **Data-level:** Systematic COVAND dataset construction with multi-modal chain-of-thought
 2065 reasoning and VQA validation, explicitly addressing spurious correlations and shortcut
 2066 learning through systematic data variation (Zheng et al., 2025; Gerych et al., 2024).
- 2067
 2068 2. **Architecture-level:** NEG-TOME’s negation-aware token merging acts as a selective
 2069 attention-head debiaser, amplifying negation-bearing tokens while suppressing spurious
 2070 features. This semantic gating follows attention-head masking principles, but operates at
 2071 the token level with learned importance weighting.
- 2072
 2073 3. **Method-level:** Strategic LoRA application to cross-modal attention layers (Sections C.3)
 2074 provides fine-grained control over negation reasoning without full model retraining, miti-
 2075 gating catastrophic forgetting associated with fine-tuning-based debiasing.
- 2076
 2077 4. **Evaluation-level:** Instance-grounded metrics that measure negation understanding sepa-
 2078 rately from general object detection, preventing bias amplification in evaluation and en-
 2079 abling fair assessment of minority negation patterns.

2080 By combining these complementary strategies, we provide stronger affirmative bias mitigation than
 2081 any single technique, addressing shortcut learning, spurious correlations, and architectural bias si-
 2082 multaneously. Furthermore, this multi-level approach generalizes beyond negation to other linguistic
 2083 phenomena requiring fine-grained compositional understanding.

2084 D ADDITIONAL ABLATIONS: NEGATION- AND NOUN-ONLY BOOSTING

2085
 2086 This section provides implementation details and empirical analysis of negation- and noun-only
 2087 boosting variants that test whether simply increasing the emphasis on certain tokens (without struc-
 2088 tural merging) is sufficient to improve negation understanding in VLM-based detectors.

2089
 2090 **Implementation details.** Given a caption string x , we first run a spaCy parser to obtain a token
 2091 sequence $d = (w_1, \dots, w_{L_{\text{spa}}})$ and phrase-level groupings P_1, \dots, P_M as described in the main
 2092 paper. We then tokenize the same string with the model’s text tokenizer (BERT/CLIP) to obtain
 2093 subword tokens $(u_1, \dots, u_{L_{\text{hf}}})$ and use the alignment procedure to map each spaCy token to its set
 2094 of subword indices.

2095 For each phrase P_i we obtain an index set $\mathcal{I}_i \subseteq \{1, \dots, L_{\text{hf}}\}$ of subword positions and compute a
 2096 merged embedding \bar{t}_i using the normalized weighted-average *merging operator*:

$$2097 \bar{t}_i = \frac{\sum_{j \in \mathcal{I}_i} \gamma_j t_j}{\sum_{j \in \mathcal{I}_i} \gamma_j}, \quad (5)$$

2098 where t_j is the original text embedding at subword index j and $\gamma_j > 0$ is an importance weight that
 2099 depends on the phrase type.

2100
 2101 In all variants, the phrase replacement is applied once per phrase: the original subword embed-
 2102 dings $\{t_j\}_{j \in \mathcal{I}_i}$ are removed and replaced by a single merged embedding \bar{t}_i at that position. The
 2103 different ablations differ only in how we choose the weights γ_j and which tokens are boosted by a
 2104 multiplicative factor $\beta > 1$:
 2105

2106 • **Noun-only Boost.** We identify head nouns inside each phrase P_i using spaCy dependency
 2107 tags (see `collect_noun_spacy_indices` and `spacy_indices_to_hf_indices`
 2108 in the code), map them to subword indices, and form a set $\mathcal{B}_{\text{noun}}$ of boosted positions. For
 2109 all phrases we use the merging operator in Eq. equation 5, with

$$2110 \quad \gamma_j = \begin{cases} \beta & \text{if } j \in \mathcal{B}_{\text{noun}}, \\ 1 & \text{otherwise.} \end{cases}$$

2111
 2112 This variant is agnostic to negation cues and only amplifies nouns/heads.

2113 • **Neg-only Boost.** We first collect spaCy indices of negation cues (“not”, “no”, “without”,
 2114 “never”, “n’t”, etc.) using `collect_negation_cue_spacy_indices`, then map them
 2115 to subword indices to obtain a set \mathcal{B}_{neg} . We again use Eq. equation 5 with

$$2116 \quad \gamma_j = \begin{cases} \beta & \text{if } j \in \mathcal{B}_{\text{neg}}, \\ 1 & \text{otherwise.} \end{cases}$$

2117
 2118 Importantly, we *do not* structurally bind the negation token to the attribute; the cue re-
 2119 mains an isolated token (or part of a short phrase) that competes with other tokens in cross-
 2120 attention.

2121 • **Merge Head Boost.** For this variant we apply phrase merging to all phrases as in Eq. equa-
 2122 tion 5, but we treat negation cues and non-negation phrases uniformly. Inside each phrase,
 2123 only the head noun is boosted:

$$2124 \quad \gamma_j = \begin{cases} \beta & \text{if } j \in \mathcal{B}_{\text{head}}, \\ 1 & \text{otherwise,} \end{cases}$$

2125
 2126 where $\mathcal{B}_{\text{head}}$ contains subword indices of phrase heads. This tests whether phrase-level
 2127 structural unification alone (without explicit negation-aware weighting) is sufficient.

2128 • **Attn Bias.** Instead of modifying the text embeddings, this variant inserts a per-token bias
 2129 into the cross-attention logits. For each negation cue index $j \in \mathcal{B}_{\text{neg}}$ we add a fixed bias
 2130 $\delta > 0$ to the attention score for that token, leaving the tokenization structure unchanged.
 2131 Concretely, if $A \in \mathbb{R}^{Q \times L_{\text{hf}}}$ is the query–key dot product matrix in a decoder block, we
 2132 replace it by $A' = A + B_{\text{neg}}$, where B_{neg} is a matrix whose j -th column is shifted by δ for
 2133 negation indices and zero elsewhere. This variant corresponds to the `Attn Bias` row in
 2134 Table S8.

2135 • **Ours (NEGToME).** For non-negated phrases P_i we use Eq. equation 5 with uniform
 2136 weights $\gamma_j = 1$, i.e., a simple average. For *negated phrases* P_{neg} that contain a negation
 2137 cue and a modified attribute (e.g., “not lying”, “without hat”) we set

$$2138 \quad \gamma_j = \begin{cases} \beta & \text{if } j \text{ corresponds to the negation cue,} \\ 1 & \text{for the other tokens in } P_{\text{neg}}. \end{cases}$$

2139
 2140 Thus, Eq. equation 5 simultaneously performs *phrase merging* and *negation-aware boost*:
 2141 all subwords in the negated phrase are collapsed into a single merged token \bar{t}_{neg} , whose
 2142 representation is dominated by the cue contribution but remains conditioned on the attribute
 2143 it negates.

2144 All variants share the same training and evaluation protocol: we fine-tune Grounding DINO-B with
 2145 LoRA on the CoVAND-L split for one epoch and evaluate on OVDEval-Negation, using COCO-
 2146 style AP and the False Positive Rate (FPR) computed after NMS.

2147 **Quantitative results.** Table S8 summarizes the results.

2148 We observe three key trends:

2149 1. **Negation-only boosting is insufficient.** The *Neg-only Boost* variant (boosting only nega-
 2150 tion cue embeddings without changing structure) yields AP = 49.7 and FPR = 62.0.
 2151 Similarly, the *Attn Bias* variant, which adds attention bias toward negation tokens while
 2152 preserving the original tokenization, collapses to the lowest AP (46.2) despite a small FPR
 2153 reduction (59.6). This confirms that simply increasing the magnitude or attention weight of
 2154 negation tokens does not translate into reliable negation understanding; it can even disrupt
 2155 compositional semantics.

2160
2161
2162
2163
2164
2165
2166
2167
2168
2169
2170
2171
2172
2173
2174
2175
2176
2177
2178
2179
2180
2181
2182
2183
2184
2185
2186
2187
2188
2189
2190
2191
2192
2193
2194
2195
2196
2197
2198
2199
2200
2201
2202
2203
2204
2205
2206
2207
2208
2209
2210
2211
2212
2213

Method	AP \uparrow	FPR \downarrow
Noun-only Boost	50.5	66.1
Neg-only Boost	49.7	62.0
Merge Head Boost	56.2	62.4
Attn Bias	46.2	59.6
Ours (NEG-TOME)	57.3	47.7

Table S8: **Negation- vs. noun-only boosting ablations on OVDEval-Negation.** All models are fine-tuned on COVAND-L for 1 epoch with identical LoRA configuration. NEG-TOME is the only variant that simultaneously improves AP and substantially reduces FPR.

- Phrase merging alone is necessary but not sufficient.** The *Merge Head Boost* variant leverages the same phrase-merging operator as NEG-TOME but boosts only the head noun in each phrase and does not treat negation cues specially. This already improves AP to 56.2, suggesting that structurally unifying multi-token phrases into single semantic units helps detection. However, FPR remains high (62.4), indicating that the model still tends to fire on both “with” and “without” queries (i.e., it detects the object but fails to respect the polarity).
- NEG-TOME (merging + negation-aware boost) is required.** Only the full NEG-TOME module, which *both* merges negation phrases and assigns a higher weight to the negation cue inside the merged representation, achieves the desired behavior: AP = 57.3 (best among all variants) and FPR = 47.7 (a reduction of 14.3–18.4 absolute points compared to the other ablations). These results support the view that the main bottleneck is not merely low attention on negation tokens, but the structural separation between cues and the attributes they modify.

Taken together, these controlled ablations provide converging evidence that (i) boosting the negation cue in isolation is not enough, and (ii) negation-aware phrase merging, as implemented by NEG-TOME, is crucial for improving both localization (AP) and negation discrimination (FPR) on OVDEval-Negation.

E COMPARISON WITH POST-HOC VQA METHODS

Motivation. An alternative to enhancing a detector’s internal negation understanding is a two-stage pipeline, where a standard detector generates initial proposals and a powerful Multimodal Large Language Model (MLLM) then acts as a post-hoc filter to remove erroneous detections. To investigate the viability and trade-offs of this common alternative, we implemented two post-hoc VQA variants. We built these on top of the same baseline detector used in our main experiments and report results on the OVDEval Negation subset using both AP and class-ignored NMS-AP.

Two post-hoc settings. (A) *Crop & Verify.* For each image, we take the detector’s top- k boxes, crop each region, and query an MLLM with a yes/no question about whether the crop satisfies the input description. This yields k separate MLLM calls per image. (B) *Coordinate Prompting.* We avoid cropping and instead pass all top- k box coordinates and the description to the MLLM at once, asking it to indicate which boxes are inconsistent.

Results. As shown in Table S9, the *Crop & Verify* method substantially increases the baseline detector’s NMS-AP from 36.8 to 54.4, confirming that a strong VQA filter can reduce contradictory detections. However, this accuracy gain comes with a heavy latency cost due to the $O(k)$ MLLM calls required per image. In contrast, the faster *Coordinate Prompting* method is unreliable for fine-grained reasoning and often degrades performance; for instance, the baseline’s NMS-AP drops from 36.8 to 34.1 when paired with the 3B verifier. Notably, our single-stage method already achieves an NMS-AP of 44.5, closing much of this performance gap without any added latency. When the accurate but slow *Crop & Verify* filter is applied on top of our already-improved model, it achieves the highest NMS-AP of 58.4, indicating that our method and post-hoc verification are complementary rather than redundant.

2214 Table S9: **Post-hoc VQA on OVDEval Negation.** Numbers are AP / NMS-AP (\uparrow). “Ours” is the
 2215 single-stage detector fine-tuned with deep-layer LoRA + NEGToME. Crop & Verify improves the
 2216 baseline but requires k MLLM calls per image; Coordinate Prompting is faster but brittle. Stacking
 2217 the expensive verifier on top of *our* improved detector yields the best overall numbers.

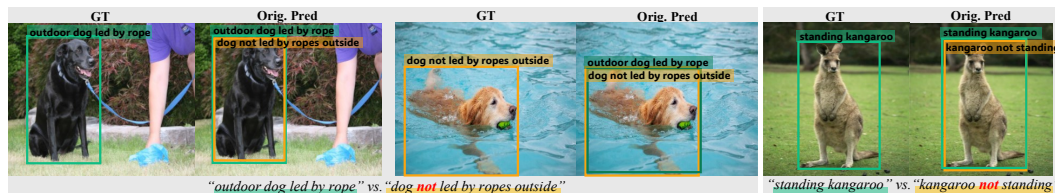
Detector	Post-hoc Verifier	AP	NMS-AP
(A) Crop & Verify (top- k crops \Rightarrow k MLLM calls)			
G-DINO-B		54.0	36.8
G-DINO-B	+ Qwen-2.5-VL-3B	59.2	54.4
G-DINO-B + Ours		58.7	44.5
G-DINO-B + Ours	+ Qwen-2.5-VL-3B	63.8	58.4
(B) Coordinate Prompting (single MLLM call with all boxes)			
G-DINO-B		54.0	36.8
G-DINO-B	+ Qwen-2.5-VL-3B	48.6	34.1
G-DINO-B	+ Qwen-2.5-VL-7B	54.0	36.9
G-DINO-B + Ours		58.7	44.5
G-DINO-B + Ours	+ Qwen-2.5-VL-3B	49.6	37.0
G-DINO-B + Ours	+ Qwen-2.5-VL-7B	58.6	44.4

2232
 2233 **Conclusion.** These experiments demonstrate that while a two-stage VQA pipeline can be effective,
 2234 it presents a clear trade-off between accuracy and speed. The crop-based verifier is accurate but slow,
 2235 whereas coordinate prompting is fast but brittle. Our single-stage approach, by contrast, instills
 2236 negation sensitivity directly within the detector, improving the stricter NMS-AP and reducing false
 2237 positives in a single, efficient pass. This confirms that post-hoc filtering does not obviate the need for
 2238 a negation-aware detector. For practical, real-time settings, integrating negation reasoning directly
 2239 into the model’s fusion layers remains the most effective path. If latency is not a concern, our work
 2240 also shows that a costly verifier can be used to further refine the outputs of our model.

2242 F EVALUATION ON FULL OVDEVAL SUBSETS

2243
 2244 OVDEval (Yao et al., 2024) is a comprehensive benchmark designed to evaluate the generalization
 2245 capability of open-vocabulary detection (OVD) models across diverse linguistic aspects. The dataset
 2246 includes 9 sub-datasets that test 6 distinct aspects: object, proper noun (landmark, logo, celebrity),
 2247 attribute (color, material), position, relationship, and negation. Each subset features meticulously
 2248 curated hard negative samples that challenge models to demonstrate true understanding of fine-
 2249 grained linguistic descriptions rather than exploiting dataset biases. For instance, the color subset
 2250 includes negative labels with the same object category but different colors, while relationship subsets
 2251 maintain identical subjects and objects but alter the connecting verbs.

2252 F.1 THE INFLATED AP PROBLEM AND NMS-AP METRIC



2254
 2255
 2256
 2257
 2258
 2259
 2260
 2261 Figure S19: Failure Cases of Prior Models on Negation Descriptions

2262
 2263 Standard Average Precision (AP) metrics face limitations when evaluating fine-grained described
 2264 object detection due to what OVDEval terms the *Inflated AP Problem*. This issue occurs when a
 2265 model predicts multiple bounding boxes for the same object with different labels, including mutu-
 2266 ally exclusive ones as in Figure S19. For example, a model might predict both “outdoor dog led
 2267 by rope” and “dog not led by ropes outside” for the same dog, artificially inflating its AP score.
 Mathematically, this manifests as:

$$\text{Precision} = \frac{TP}{TP + FP} = \frac{1}{1 + 1} = 0.50, \quad \text{Recall} = \frac{TP}{GT_{num}} = \frac{1}{1} = 1.0 \quad (6)$$

Where a model with no actual understanding of attributes can still achieve a mAP of 0.50. To address this, we follow OVDEval’s Non-Maximum Suppression Average Precision (NMS-AP) metric (Yao et al., 2024), which applies class-ignored NMS to remove redundant predictions for the same object before AP calculation. This provides a more accurate assessment of a model’s ability to understand fine-grained descriptions of contradictory pairs.

F.2 GENERALIZATION TO NON-NEGATION SUBSETS

Table S10 demonstrates that our model maintains robust performance across all OVDEval subsets despite being trained exclusively on the negation-focused COVAND dataset. Notably, our approach shows improved NMS-AP scores for Logo (+0.2), Landmark (+4.8), Color (+0.7), and Relationship (+3.8) subsets compared to the baseline. This broad generalization suggests that our negation-sensitive adaptations enhance the model’s overall reasoning capabilities for complex descriptions. These results confirm that our LoRA-based parameter-efficient fine-tuning and NEGTOme token merging strategy provide benefits beyond negation understanding, enhancing the model’s capability to process compositional descriptions across multiple semantic aspects.

Table S10: **Evaluation Results on Full OVDEval.** Performance on OVDEval subsets, except for the Negation. Even though we only trained with negation-focused COVAND dataset, our models show robust results for other subsets.

	Logo		Landmark		Celebrity		Color		Material		Position		Relationship		Average	
	AP	NMS-AP	AP	NMS-AP	AP	NMS-AP	AP	NMS-AP	AP	NMS-AP	AP	NMS-AP	AP	NMS-AP	AP	NMS-AP
G-DINO	11.7	7.6	20.5	16.5	6.7	0.8	7.9	5.6	15.2	5.5	74.7	60.6	41.3	18.3	25.4	16.4
+Ours	11.5	7.8	22.4	21.3	6.6	0.3	7.9	6.3	15.8	5.3	70.5	54.6	42.3	22.1	25.2	16.8

G ANALYSIS ON RPN-BASED DETECTOR

G.1 LIMITATIONS OF RPN-BASED DETECTORS UNDER NEGATION

Marginal or negative gains with LoRA. Two-stage region-proposal detectors such as GLIP (Li et al., 2022) and FIBER (Dou et al., 2022) obtain slight improvement on negation-focused benchmarks after attaching LoRA adapters as in Table S11. For GLIP, whose backbone consists of stacked multi-head attention blocks, we inject LoRA only into the FFN layers of the last two transformer blocks, leaving all attention projections frozen. Even with this targeted fine-tuning, the gains remain marginal. These findings indicate that low-rank fine-tuning brings far smaller gains to GLIP than to DETR-style detectors. The gap can be traced to their attention layouts: GLIP employs self-MHA over a mixed token pool, whereas Grounding-DINO uses two modality-specific cross-attention blocks driven by a compact query set, a design that lets LoRA and NEGTOme act directly on phrase-level cues and thus respond much more strongly to negation.

Affirmative bias and context insensitivity. Recent negation benchmarks reveal a sharp drop in detection accuracy whenever a query expresses absence or negation (Alhamoud et al., 2025). GLIP and FIBER often treat a negated phrase (“not X”) as if it were “X”, triggering on object names while ignoring context qualifiers. Consequently, GLIP still localizes a “microphone” when the description states “a person with no microphone”, producing hallucinated objects. LoRA-adapted RPN detectors exhibit diminishing returns on negation-centric tasks because their proposal stage detects any region matching a noun, leaving little capacity to encode absence semantics.

Performance gap between AP and NMS-AP on the Negation subset. Table S11 further shows that model capacity alone does not resolve the issue: even the larger GLIP-L still exhibits a gap between AP and class-ignored NMS-AP, substantially wider than the gap of smaller DETR counterparts. The gap quantifies how many redundant, mutually exclusive boxes each model produces.

A large drop after class-ignored NMS indicates that the detector continues to fire on the noun even when the query contains a negation cue, confirming the affirmative bias analyzed in the main paper.

Effect of NEGToME. DETR keeps token granularity throughout the vision–language stack, allowing a merged phrase embedding to dominate $\langle q, k_i \rangle$ for its specific key k_i while leaving other keys unaltered. By contrast, GLIP or FIBER fuse language either by (a) global pooling of the entire caption (`[cls]`), or (b) class-name pooling plus a separate visual prompt. Both strategies erase intra-sentence polarity (*dog* vs. *not dog*) before the detector sees it. Token merging cannot recover that lost contrast; at best it shortens a sequence that will be pooled anyway.

Table S11: **OVDEval-Negation Evaluation on Additional Architectures.** RPN-based detectors show a large gap between AP and NMS-AP. FT denotes fine-tuning of LoRA parameters only, with all other pretrained weights kept frozen as in the main paper. Results marked with † are reproduced.

	Image Backbone	Total Param.	AP	NMS-AP (Yao et al., 2024)
<i>Non RPN-based Detector</i>				
MDETR (Kamath et al., 2021)	ResNet-101	185M	41.1	28.3
OmDet (Zhao et al., 2024b)	ConvNext-B	242M	55.9	35.1
Grounding DINO† (Liu et al., 2024b)	Swin-B	233M	54.0	36.8
<i>RPN-based Detector</i>				
FIBER (Dou et al., 2022)	Swin-B	252M	57.2	28.7
GLIP-L (Li et al., 2022)	Swin-L	430M	51.8	29.3
GLIP-T (Li et al., 2022)	Swin-T	232M	47.7	25.4
+ FT w. CoVAND			47.8	26.1
+ FT w. CoVAND + NEGToME			48.3	26.0

G.2 ADVANTAGES OF DETR–STYLE DETECTORS WITH LoRA

Compositional reasoning. DETR-style detectors with transformer decoders (Kamath et al., 2021; Liu et al., 2024b; Li et al., 2023; Shen et al., 2024) perform joint text–image reasoning through cross-attention in decoder blocks. This design enables natural handling of relations such as “*X but not Y*”.

Effectiveness of LoRA. Injecting LoRA adapters into the decoder cross-attention layers of Grounding DINO and fine-tuning on a negation-focused dataset improves mAP by +2.6 and cuts the false positive rate by 11.5%. The same lightweight adaptation reduces spurious detections on the Negation subset of OVDEval by nearly half, while preserving general detection accuracy.

Why the architecture helps. Each decoder layer attends to textual tokens; negation words therefore, modulate visual attention directly. In RPN pipelines, language supervision is applied only after proposals are fixed, limiting early rejection of forbidden objects. A fully fused DETR decoder yields a contextual representation of “what *not* to detect,” which a small LoRA module can efficiently refine.

Advantage of NEGToME. Both Grounding DINO and APE inherit the sub-token fragmentation of their text backbones with BERT and BPE in CLIP. NEGToME merges those fragments into one polarity-aware phrase embedding and re-weights it by a boost factor β . In Grounding DINO, this merged vector is fed intact through token-level cross-attention, so every decoder layer receives a sharper gradient signal for the absence condition; the result is a +10.8 rise in NMS-AP and a 19.1% drop in false positives on OVDEval-Negation. APE employs CLIP, whose text encoder pools all tokens into a single sentence vector before fusion. Here NEGToME acts pre-pooling: by assigning larger softmax weights to the merged negation phrase it skews the sentence representation toward the correct polarity, yet does not increase sequence length. Consequently, the lightweight merger lifts APE-Ti by +1.2 in NMS-AP and reduces absent-object errors by 8.3%, despite updating only 0.017% of parameters. NEGToME aligns with the inductive bias of both encoders: it supplies BERT-based decoders with an explicit token for cross-modal attention, and it biases CLIP’s global pooling toward the correct semantic polarity. The mechanism is encoder-agnostic and therefore complements LoRA across heterogeneous DETR frameworks.

2376 DETR-based detectors fine-tuned with LoRA and NEGTOPE achieve larger and more reliable gains
 2377 on negation and other compositional queries than RPN counterparts. Their set-prediction decoder
 2378 offers a single, expressive locus for parameter-efficient language adaptation.
 2379

2380 H ZERO-SHOT DOWNSTREAM TASKS: MULTIPLE CHOICE QUESTIONS 2381

2382
 2383 To further analyze our model’s semantic comprehension of negation, we evaluate it on the NegBench
 2384 Multiple Choice Question (MCQ) benchmark (Alhamoud et al., 2025). This benchmark is specif-
 2385 ically designed to diagnose a VLM’s ability to handle negation by requiring it to select the most
 2386 accurate caption for an image from four options. These options are structured into three challenging
 2387 categories as detailed below, providing a fine-grained analysis of a model’s capabilities.
 2388

2389 H.1 STRUCTURE OF THE NEGBENCH MCQ 2390

2391 The NegBench MCQ task (Alhamoud et al., 2025) generates multiple-choice questions where one
 2392 answer is correct and the other three serve as hard negatives, designed to mislead models that do not
 2393 properly understand negation. The questions are categorized into three distinct types based on the
 2394 linguistic structure of the correct answer:

- 2395 • **Positive Subset:** The correct caption is a simple affirmation that accurately describes ob-
 2396 jects present in the image (e.g., “*This image shows a baseball bat and baseball glove*”).
 2397 This subset tests the model’s fundamental visual grounding capabilities, as shown in Fig-
 2398 ure S20. Incorrect options often involve falsely negating a present object.
- 2399 • **Negative Subset:** The correct caption accurately negates the presence of an object that is
 2400 contextually relevant but absent from the image (e.g., “*A bowl is not present in this image*”).
 2401 This directly tests the model’s ability to comprehend explicit negation, as illustrated in
 2402 Figure S21.
- 2403 • **Hybrid Subset:** The correct caption combines both an affirmation and a negation within a
 2404 single sentence (e.g., “*This image features a person, with no truck in sight*”). As shown in
 2405 Figure S22, this is the most challenging subset as it requires compositional reasoning and
 2406 an understanding of complex sentence structures that assign different polarities to different
 2407 objects.
 2408

2409 H.2 ERROR PATTERN ANALYSIS OF BASELINE MODELS 2410

2411 Our qualitative analysis reveals that baseline models exhibit consistent and fundamental error pat-
 2412 terns on the NegBench MCQ task, primarily stemming from a severe *affirmative bias* as below:
 2413

- 2414 1. **Blatant Contradiction of Visual Facts:** The most common failure is choosing a caption
 2415 that directly contradicts the visual evidence. For example, in Figure S21, the baseline
 2416 model selects “*There is no horse in this image*” for an image clearly depicting a horse. This
 2417 indicates that the model heavily weighs the noun (“*horse*”) while effectively ignoring the
 2418 negation cue, treating both affirmative and negative statements as semantically similar.
- 2419 2. **Polarity Confusion in Hybrid Sentences:** In the Hybrid subset (Figure S22), baseline
 2420 models systematically fail to parse sentences containing both positive and negative clauses.
 2421 For instance, given the ground truth “*This image features a refrigerator, but lack of a bottle,*”
 2422 the baseline chooses “*This image features a bottle, but does not include a refrigerator.*”
 2423 This shows a critical failure in compositional reasoning, where the model cannot correctly
 2424 assign presence and absence to different objects within the same logical construct.
- 2425 3. **Selection of Suboptimal Negatives:** In some cases on the Negative subset, the baseline
 2426 avoids direct contradiction but fails to select the most accurate description. As seen in
 2427 Figure S21, when the ground truth is “*A bowl is not present,*” the baseline chooses “*no*
 2428 *cake is present.*” While factually correct, this choice suggests the model lacks a deeper
 2429 contextual understanding to identify the most salient absent object among multiple true
 negative options.

2430 These error patterns underscore that many state-of-the-art VLMs do not understand negation. In-
 2431 stead, they rely on shortcut strategies that collapse the semantic meaning of affirmative and negative
 2432 statements. This motivates the need for methods that can fundamentally address this architectural
 2433 limitation.

2434
 2435
 2436
 2437

2438
 2439
 2440
 2441
 2442
 2443
 2444
 2445



- ✔ (1) This image shows a baseball bat and baseball glove
- (2) This image features a dining table, but does not include a baseball bat.
- (3) A dining table is present in this image.
- (4) This image doesn't feature a baseball bat

2446
 2447
 2448
 2449
 2450
 2451
 2452
 2453



- ✔ (1) This image features both a zebra and a giraffe.
- (2) A cow is present in this image, but there is no zebra.
- (3) A cow is present in this image.
- (4) No zebra is present in this image.

2454
 2455
 2456
 2457
 2458
 2459
 2460
 2461



- ✔ (1) This image features a knife and a dining table.
- (2) This image contains a bowl, with no knife in sight.
- (3) This image shows a bowl.
- (4) Noticeably absent from this image is a knife.

2462
 2463
 2464
 2465
 2466
 2467
 2468
 2469
 2470
 2471
 2472
 2473
 2474
 2475
 2476
 2477
 2478
 2479
 2480
 2481
 2482
 2483

Figure S20: Qualitative Results on the Positive subset of the Multiple Choice Question benchmark. Captions with green checkmark ✔ is GT, pink refer to Baseline, and blue refer to Ours.

2484
2485
2486
2487
2488
2489
2490
2491
2492
2493
2494
2495
2496
2497
2498
2499
2500
2501
2502
2503
2504
2505
2506
2507
2508
2509
2510
2511
2512
2513
2514
2515
2516
2517
2518
2519
2520
2521
2522
2523
2524
2525
2526
2527
2528
2529
2530
2531
2532
2533
2534
2535
2536
2537

	<p>✓(1) A bowl is not present in this image.</p> <p>(2) This image features a bowl, but no cake is present.</p> <p>(3) A bowl is shown in this image.</p> <p>(4) No cake is included in this image.</p>
	<p>✓(1) This image contains no car.</p> <p>(2) This image shows a car, but no horse is present.</p> <p>(3) This image features a car.</p> <p>(4) There is no horse in this image.</p>
	<p>✓(1) There is no chair in this image.</p> <p>(2) This image features a chair, but there's no cat.</p> <p>(3) A chair is present in this image.</p> <p>(4) There is no cat in this image.</p>
	<p>✓(1) There is no traffic light in this image.</p> <p>(2) This image features a traffic light, but no car is present.</p> <p>(3) A traffic light is included in this image.</p> <p>(4) No car is present in this image.</p>

Figure S21: **Qualitative Results on the Negative subset of the Multiple Choice Question benchmark.** Captions with green checkmark ✓ is GT, **pink** refer to **Baseline**, and **blue** refer to **Ours**.

2538
2539
2540
2541
2542
2543
2544
2545
2546
2547
2548
2549
2550
2551
2552
2553
2554
2555
2556
2557
2558
2559
2560
2561
2562
2563
2564
2565
2566
2567
2568
2569
2570
2571
2572
2573
2574
2575
2576
2577
2578
2579
2580
2581
2582
2583
2584
2585
2586
2587
2588
2589
2590
2591

	<ul style="list-style-type: none">✓(1) This image features a refrigerator, but lack of a bottle.(2) This image features a bottle, but does not include a refrigerator.(3) A bottle is included in this image.(4) A refrigerator is not present in this image.
	<ul style="list-style-type: none">✓(1) This image includes a sheep but no truck.(2) This image shows a truck, but there is no sheep.(3) This image shows a truck.(4) There is no sheep in this image.
	<ul style="list-style-type: none">✓(1) This image features a dining table, but no car is present.(2) This image features a car, but does not include a dining table.(3) A car is included in this image.(4) A dining table is not included in this image.
	<ul style="list-style-type: none">✓(1) This image features a frisbee, but there's no bench in sight.(2) This image features a bench, but no frisbee is visible.(3) This image shows a bench.(4) A frisbee is not included in this image.

Figure S22: Qualitative Results on the Hybrid subset of the Multiple Choice Question benchmark. Captions with green checkmark ✓ is GT, pink refer to Baseline, and blue refer to Ours.

I QUALITATIVE RESULTS

We present additional qualitative examples from the OVDEval and D³ datasets to further demonstrate the effectiveness of our negation understanding approach. Figure S23 and Figure S24 show our model’s ability to distinguish between contradictory attribute pairs such as “horse urinating” versus “horse that is not urinating” and “complete pizza” versus “pizza that is not complete”. The baseline model often detects identical regions for both negative and positive descriptions, demonstrating significant affirmative bias. In contrast, our method successfully differentiates between these contradictory descriptions by correctly emphasizing negation cues.

Figures S25 to S27 illustrate our model’s performance on the D³ dataset. For descriptions such as “hanger without clothes” and “a bed without patterns”, our model correctly identifies only the objects that satisfy these negated constraints. The baseline frequently exhibits false positives by detecting objects regardless of negation markers. Our approach demonstrates particular effectiveness for simple negation cases involving physical attributes and object presence.

Despite these improvements, our method still exhibits limitations in scenarios requiring highly complex reasoning, as shown in Figure S28. These challenges often involve multi-step relational logic combined with negation, such as in the query “a woman in white wedding dress not beside any men in suits”, or understanding negated states, as in “a volley ball in the middle of the air untouched”. Furthermore, resolving ambiguous or implicit negation cues like “unlike” in “origami unlike bird” remains a difficult problem. A common failure pattern in these cases is that when a complex event or state is entirely absent from the image (e.g., “the person who was proposed to on one knee”), the model defaults to its affirmative bias, detecting the main subject of the query (“person”) rather than correctly identifying that no object matches the full description. Crucially, the baseline model faces identical challenges in these cases, demonstrating that these are open problems for the current generation of VLM detectors. This confirms that our method, while not a complete solution for such intricate reasoning, does not degrade performance on these hardest examples. These limitations highlight important areas for future research in handling complex linguistic constructions and multi-step negation scope resolution.

J DECLARATIONS

LLM usage. A large language model (LLM) was used during the preparation of this paper to proofread and refine the writing, including correcting grammar and improving sentence structure.

Ethics Statement. Our work adheres to the ICLR Code of Ethics. The primary goal of this research is to improve the reliability and safety of vision-language models by addressing a fundamental flaw in their reasoning—the failure to understand negation. By reducing “affirmative bias,” we aim to create models that align more closely with human language and intent, which can prevent critical errors in real-world applications (e.g., medical imaging or autonomous systems). Our new dataset, COVAND, is built upon the public Flickr30k Entities benchmark. The new captions are generated using a large language model (GPT-4o) with a systematic, multi-step pipeline designed to ensure high-quality, relevant, and grounded annotations. While our method improves a model’s linguistic comprehension, it does not inherently address or remove societal biases that may be present in the underlying web-scale pre-training data or the baseline models themselves. We believe the contribution is a net positive, leading to more robust and predictable AI systems.

Reproducibility Statement. We are committed to ensuring the reproducibility of our research. To this end, we will make our source code, including the implementation of the NEGTOPE module, and the complete COVAND dataset publicly available upon publication.



Figure S23: **Qualitative Results on OVDEval Datasets (1)**. Prediction results on contradictory caption pairs (yellow box vs. green box) from the negation subset of OVDEval dataset. Each row displays (left) ground-truth boxes, (middle) baseline predictions, and (right) our predictions. Our model effectively reduces affirmative bias, no longer returning identical bounding boxes for captions that express opposite meanings.

2700
 2701
 2702
 2703
 2704
 2705
 2706
 2707
 2708
 2709
 2710
 2711
 2712
 2713
 2714
 2715
 2716
 2717
 2718
 2719
 2720
 2721
 2722
 2723
 2724
 2725
 2726
 2727
 2728
 2729
 2730
 2731
 2732
 2733
 2734
 2735
 2736
 2737
 2738
 2739
 2740
 2741
 2742
 2743
 2744
 2745
 2746
 2747
 2748
 2749
 2750
 2751
 2752
 2753



Figure S24: **Qualitative Results on OVDEval Datasets (2)**. Prediction results on contradictory caption pairs (yellow box vs. green box) from the negation subset of OVDEval dataset. Each row displays (left) ground-truth boxes, (middle) baseline predictions, and (right) our predictions. Our model effectively reduces affirmative bias, no longer returning identical bounding boxes for captions that express opposite meanings.

2754
2755
2756
2757
2758
2759
2760
2761
2762
2763
2764
2765
2766
2767
2768
2769
2770
2771
2772
2773
2774
2775
2776
2777
2778
2779
2780
2781
2782
2783
2784
2785
2786
2787
2788
2789
2790
2791
2792
2793
2794
2795
2796
2797
2798
2799
2800
2801
2802
2803
2804
2805
2806
2807

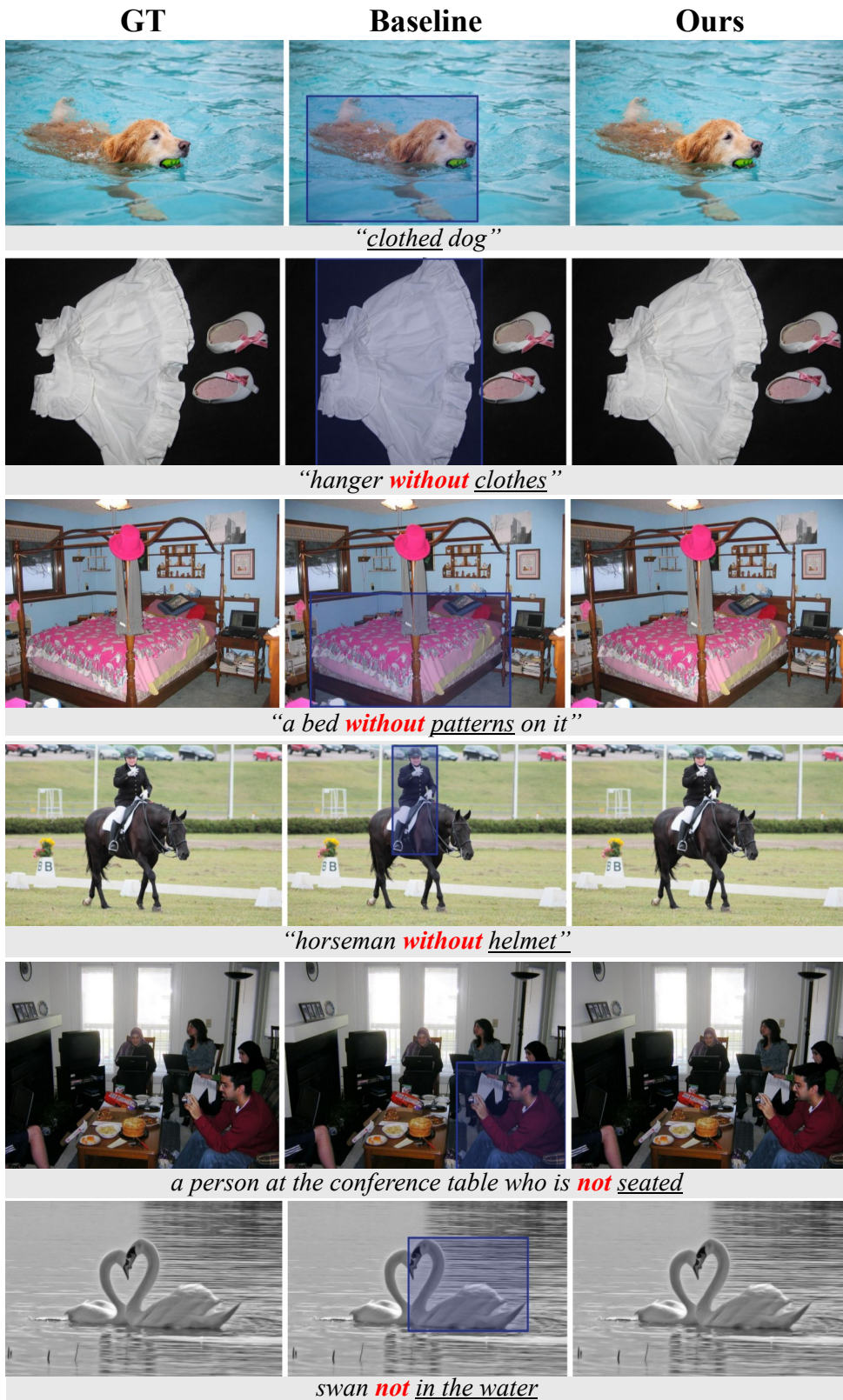


Figure S25: **Qualitative Results on D³ Datasets (1)**. Absence of a bounding box shows the model has determined that no instance in the image matches the input description. By filtering out such invalid predictions, our approach reduces affirmative bias and lowers the false-positive rate.

2808
2809
2810
2811
2812
2813
2814
2815
2816
2817
2818
2819
2820
2821
2822
2823
2824
2825
2826
2827
2828
2829
2830
2831
2832
2833
2834
2835
2836
2837
2838
2839
2840
2841
2842
2843
2844
2845
2846
2847
2848
2849
2850
2851
2852
2853
2854
2855
2856
2857
2858
2859
2860
2861



Figure S26: **Qualitative Results on D³ Datasets (2)**. Absence of a bounding box means the model has determined that no instance in the image matches the input description. Our model effectively reduces the affirmative bias while keeping the correct predictions.

2862
2863
2864
2865
2866
2867
2868
2869
2870
2871
2872
2873
2874
2875
2876
2877
2878
2879
2880
2881
2882
2883
2884
2885
2886
2887
2888
2889
2890
2891
2892
2893
2894
2895
2896
2897
2898
2899
2900
2901
2902
2903
2904
2905
2906
2907
2908
2909
2910
2911
2912
2913
2914
2915

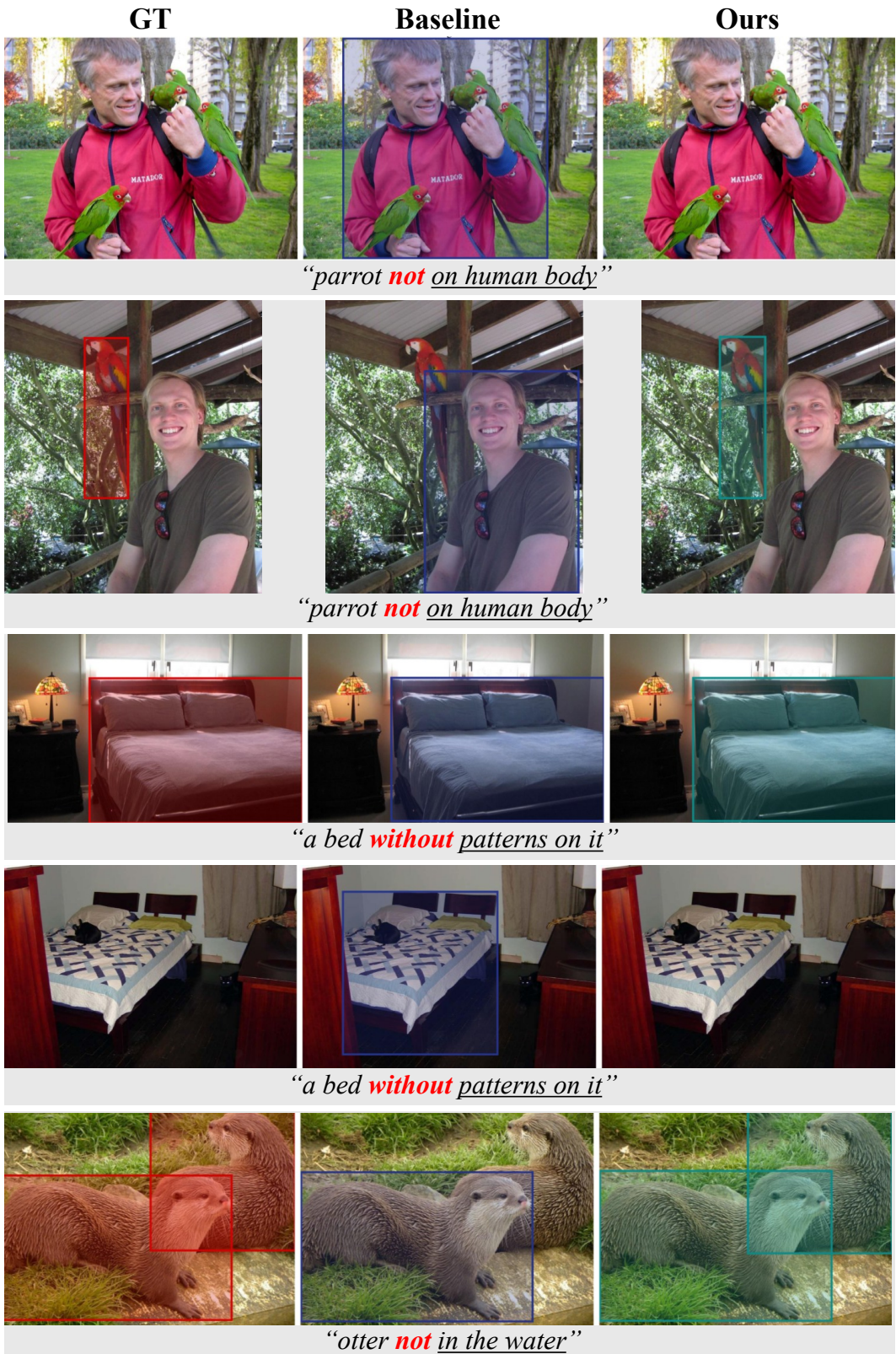


Figure S27: **Qualitative Results on D³ Datasets (3)**. Absence of a bounding box means the model has determined that no instance in the image matches the input description. Our model effectively reduces the affirmative bias while keeping the correct predictions.

2916
2917
2918
2919
2920
2921
2922
2923
2924
2925
2926
2927
2928
2929
2930
2931
2932
2933
2934
2935
2936
2937
2938
2939
2940
2941
2942
2943
2944
2945
2946
2947
2948
2949
2950
2951
2952
2953
2954
2955
2956
2957
2958
2959
2960
2961
2962
2963
2964
2965
2966
2967
2968
2969

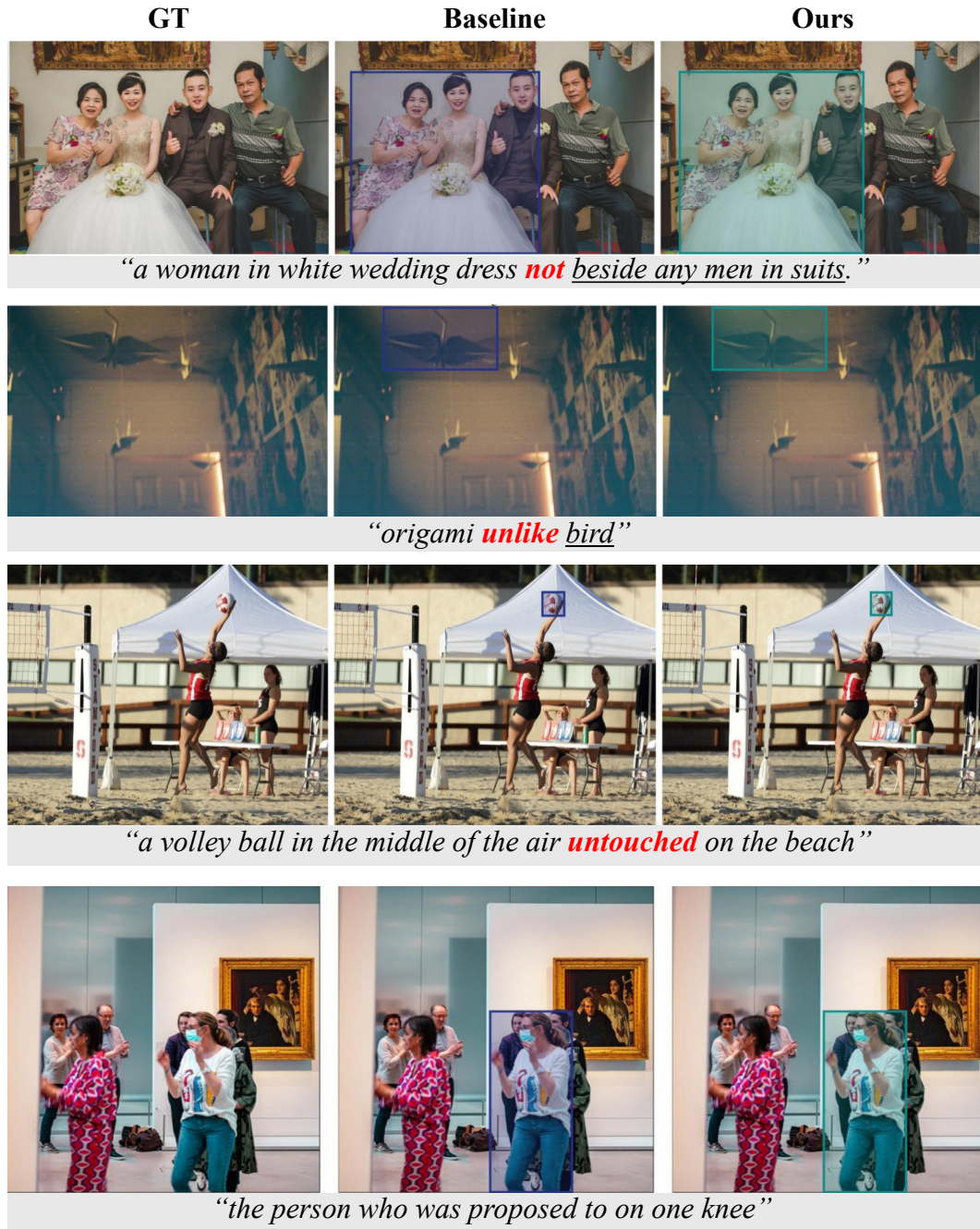


Figure S28: **Qualitative Analysis of Limitations on Complex Negation.** Despite overall improvements, our method, like the baseline, still struggles with highly complex linguistic constructions involving negation. The examples show failures in: (i) multi-step relational reasoning (“not beside any men in suits”), (ii) abstract or implicit negation (“unlike bird”), (iii) understanding negated states (“untouched”), and (iv) recognizing the absence of a complex event (“proposed to on one knee”). In these challenging cases, both models tend to default to their affirmative bias, detecting the main subject of the query rather than correctly concluding that nothing in the image matches the full description. These limitations highlight the need for more sophisticated compositional reasoning to ground complex negative constraints.